Automated Three-Dimensional Image Segmentation of Retinal OCT Images

Narendra Patel

A Dissertation Submitted to
Indian Institute of Technology Hyderabad
In Partial Fulfillment of the Requirements for
The Degree of Master of Technology

भारतीय प्रौद्योगिकी संस्थान हैदराबाद
Indian Institute of Technology Hyderabad

Department of Biomedical Engineering

July, 2014

Declaration

I declare that this written submission represents my ideas in my own words, and where others' ideas or words have been included, I have adequately cited and referenced the original sources. I also declare that I have adhered to all principles of academic honesty and integrity and have not misrepresented or fabricated or falsified any idea/data/fact/source in my submission. I understand that any violation of the above will be a cause for disciplinary action by the Institute and can also evoke penal action from the sources that have thus not been properly cited, or from whom proper permission has not been taken when needed.
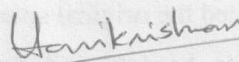
_____

(-Signature-)

Narendra Patel

(-Student Name-)

BM12M1002

(-Roll No.-)

ii

Approval Sheet

This thesis entitled – Automated Three-Dimensional Image Segmentation of Retinal OCT Images – by – Narendra Patel – is approved for the degree of Master of Technology from IIT Hyderabad.
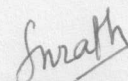
Dr. Harikrishnan Narayanan Unni

Assistant professor, Department of Biomedical Engineering

Indian Institute of Technology Hyderabad

Examiner

Dr. Subha Narayan Rath

Assistant professor, Department of Biomedical Engineering

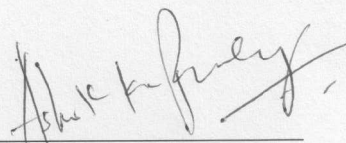Indian Institute of Technology Hyderabad

Examiner

Dr. Renu John

Assistant professor, Department of Biomedical Engineering

Indian Institute of Technology Hyderabad

Adviser

Dr. Ashok Kumar Pandey

Assistant professor, Department of Mechanical Engineering

Indian Institute of Technology Hyderabad

Chairman

iii

Acknowledgements

Dedicated to

My Family and Friends

Abstract

Optical coherence tomography (OCT) has become an essential tool in ophthalmology. The macular OCT images are three dimensional, high resolution and cross-sectional image of macula, which provides detailed structural information of various macular layers. Moreover macular OCT imaging is non-contact, non-invasive and real-time. OCT images can be obtained quickly and multiple times, this allows easy diagnosis and treatment progress monitoring. With advances in technology acquired dataset size is also increasing, which makes it impractical to manually segment macular layers in clinical environment. Thus need of fast and accurate segmentation algorithm is ever increasing. In this thesis two segmentation algorithms have been developed. The two-dimensional segmentation algorithm based on gradient method successfully marked three retinal layers and five layer boundaries. The three-dimensional segmentation algorithm is based on threshold and characteristic intensity profile of macular OCT scan. The gradient method is well suited for boundary detection where large changes in intensity occur.

With 3-D segmentation process utilizing intensity and location information of layers, 11macular boundaries were successfully obtained. Three dimensional processing reduced the errors caused by shadows due to blood vessels. Moreover processing time and memory requirement of computer system was significantly reduced by limiting search region in macular part of image and removing the vitreous and choroid region. Uniform intensity variation in each A-scan throughout macula was obtained by 3-D filtering and normalization. This helped in generalizing the search parameters for various layers and layer boundaries. The segmentation process was further simplified by intensity based partitioning of the macula in three regions.

Nomenclature

OCT: Optical Coherence Tomography

TD-OCT: Time Domain Optical Coherence Tomography

SD-OCT: Spectral Domain Optical Coherence Tomography

FD-OCT: Fourier Domain Optical Coherence Tomography

ILM: Inner Limiting Membrane

IPL: Inner Plexiform Layer

INL: Inner Nuclear Layer

OPL: Outer Plexiform Layer

ONL: Outer Nuclear Layer

ELM: External Limiting Membrane

IS/OS: Junction of Inner and Outer Photoreceptor Segments

OPR: Outer Segment PR/RPE Complex

NFL: Nerve Fiber Layer

GCL: Ganglion Cell Layer

RPE: Retinal Pigment Epithelium

BM: Bruch's Membrane

CSCR: Central Serous Chorioretinopathy

Contents

List of Figures

List of Tables

Chapter 1
Introduction

1.1   Background

Optical coherence tomography (OCT) is now a standard tool for diagnosis of ocular diseases. Among other ophthalmic imaging techniques such as scanning laser polarimetry and confocal scanning ophthalmoscope, OCT has become favorite tool for ocular imaging because of the wide variety of information it provides. OCT provides micron level cross-sectional and three dimension visualization of tissue structures. OCT imaging is non-contact, noninvasive and real-time. Fast imaging, without need of tissue preprocessing makes it first choice for diagnosis and treatment progression monitoring of macular diseases and glaucoma. Advancement in technology is increasing axial and transverse resolution and decreasing image acquisition time. OCT imaging is based on low coherence interferometry. OCT uses a broadband light source to scan tissue and low coherence interferometry is used to detect the magnitude and time delay of backscattered light. The three dimensional visualization of tissue is obtained by scanning light beam on tissue surface using dual axis galvanometer optical scanners. Unlike other microscopy techniques, the axial resolution does not depend upon the aperture size, but on coherence length of light source. This unique feature enables OCT system to image deep retinal tissue and can be combined with wide range of instruments such as catheter, endoscopes and probes.

1.2   Motivation

Optical coherence tomography is an essential tool for noninvasive assessment of variety of ocular diseases such as glaucoma, age related macular degeneration and diabetic retinopathy. Previously OCT machines performed time domain imaging. TD-OCT imaging was slower in image acquisition; few scans approximately 6 were imaged in one in each scan to reduce motion artifacts due to eye movement. Manual marking of retinal layers and analysis of few images could be performed in clinics. But with introduction of new spectral domain optical coherence tomography image resolution and acquisition speed has improved drastically. A SD-OCT scan of dimension 1024×512×128 can be obtained in 1.6 seconds at scanning rate of 27000 A-scans per second[1]. Manual analysis and marking of various retinal layers in such large data set acquired by SD-OCT is not practical in clinical environment. There is need of three dimensional, automatic and fast OCT image segmentation technique to exploit the advances in OCT imaging modality.

1.3   Contribution of the Thesis

The primary objective of this work is to perform three-dimensional automated segmentation of retinal layers in retinal spectral domain optical coherence tomography images. Two segmentation algorithms based on gradient and threshold using image profile of macular

image were developed. The gradient based segmentation performed better only for few layers where sharp change in intensity level occurs, such as at ILM, IS-OS, RPE-choroid and OPL-ONL.

The three-dimensional segmentation algorithm based on threshold along with the intensity profile of macular layer and location information of various layers, eleven macular boundaries were successfully segmented. The processing time and memory requirement of computer system was significantly reduced by limiting segmentation process only in macular region and rejecting the large space occupied by vitreous and choroid region. The macular OCT image segmentation process is simplified and generalized by dividing the macular cube into three regions and homogenized intensity variation in macular cube using 3-D filtering and A-scan normalization.

1.4   Organization of the Thesis

The thesis is organized as follows:

Chapter 2: provides an overview of optical coherence tomography technology and various methods of retinal OCT image segmentation.

Chapter 3: presents introduction to human eye anatomy and various pathologies of eye where OCT imaging is useful.

Chapter 4: in this chapter, macular OCT image segmentation algorithms have been described.

Chapter 5: contains summary of segmentation algorithms with conclusion and future work.

Chapter 2
Optical Coherence Tomography and Image Segmentation

2.1   Introduction to Optical Coherence Tomography

Optical coherence technology (OCT) is a high resolution 3 dimensional imaging technology. OCT can generate 3 dimensional images of biological tissue structures noninvasively at micron scale resolution by measuring their optical reflection. OCT is similar to ultrasound, but it measures intensity of backscattered light instead of acoustic wave. OCT image resolution of 1 to 15 micron makes it suitable for visualization of tissue morphology. OCT image acquisition is fast and highly reproducible. OCT images can be obtained in real time, which allows tissue microstructure visualization without excision or preprocessing of specimen as required in conventional histopathology or biopsy.

The most essential part of OCT is Michelson's interferometer. An optical signal that is transmitted through or reflected from a biological tissue will contain time-of-flight information, which in turn gives spatial information about tissue microstructures [2].

OCT has become a standard diagnostic technique for retinal diseases and glaucoma [3]. OCT can also be performed along with wide variety of instruments such as catheter, needle, small endoscope, ophthalmoscope, probes or any other surgical instruments. OCT is an emerging technology for intravascular imaging where it can identify unstable plaques that are prone to rupture, producing myocardial infarction [4]. OCT is combination of multiple technologies including photonics, high speed electronics and signal processing, imaging processing, medical device development and biomedical engineering [5].

2.2   History

Optical coherence tomography has become an essential tool for noncontact noninvasive in situ analysis of retina for diagnosis and monitoring of retinal diseases and glaucoma. First OCT images of retina and coronary artery ex vivo were reported in 1991 [2]. The ocular imaging with prototype OCT system started in 1994 and the OCT technology was patented and transferred to Carl Zeiss Meditec, Inc. Based on Time-Domain OCT technology, first OCT system "OCT 1000" was commercially available in 1996. Further improved version "OCT 2000" and "Stratus OCT" were introduced in year 2000 and 2002. Stratus OCT became gold standard in Time Domain OCT systems. In a major breakthrough in OCT technology, Spectral Domain/ Fourier Domain OCT was introduced in 2006. SD/FD OCT has higher resolution and fast scanning speed over TD-OCT. Current commercially available SD-OCT systems for retinal imaging has resolution of 5 microns and scanning speed of 27,000 A-scans per second. Ultra high speed (70,000 – 315,000 axial scans per second) and high resolution (2.5 – 8μm) imaging at 850 nm was demonstrated with new CMOS line scan sensor technology [6].

2.3   Principle

Optical coherence tomography is an interferometry based imaging modality. The heart of OCT is a Michelson interferometer. Figure 2.1 shows the schematic of Michelson interferometer. OCT is similar to Ultrasound imaging with acoustic energy replaced by infrared beam. Biological specimen / material are scanned using Infrared light beam. The backscattered / backreflected light from sample contains information on time-of-flight delay from the reflective boundaries and backscattering sites in the sample. The intensity of backscattered light is recorded simultaneously with position of scanning and scaled logarithmically to form a black and white or false color image for better understanding.

In ultrasound imaging echo time of acoustic wave is detected. The velocity of acoustic wave and light in water is 1.5×10^3 meter per second and 3×10^8 meter per second respectively. The spatial/ distance information and echo time delay relation can be shown by formula $\Delta T=z/v$; where ΔT is echo time, z is the distance travelled, and v is velocity. For resolution of 100 microns in typical ultrasound imaging echo time delay is approximately 100 nanoseconds. But for a resolution of 10 microns in OCT imaging, time resolution is 30fsec (30×10^{-15}).

OCT performs low coherence interferometry for detecting magnitude and time delay of backscattered light. In Low coherence interferometry echo time delay and intensity of backscattered light is measured by interfering with a light that has travelled a known reference path and time delay. The light from a low coherence light source is split into two arms of interferometer i.e. sample arm and reference arm. The light beam in sample arm is directed and scanned on the sample. The reference arm contains scanning delay line to control the path length and thus control axial focus point in sample being imaged. The backscattered light from sample arm is interfered with light from reference arm and this interference pattern is detected using photo-detector. Constructive interference will happen only when the two light beams in reference arm and sample arm have travelled equal distance.
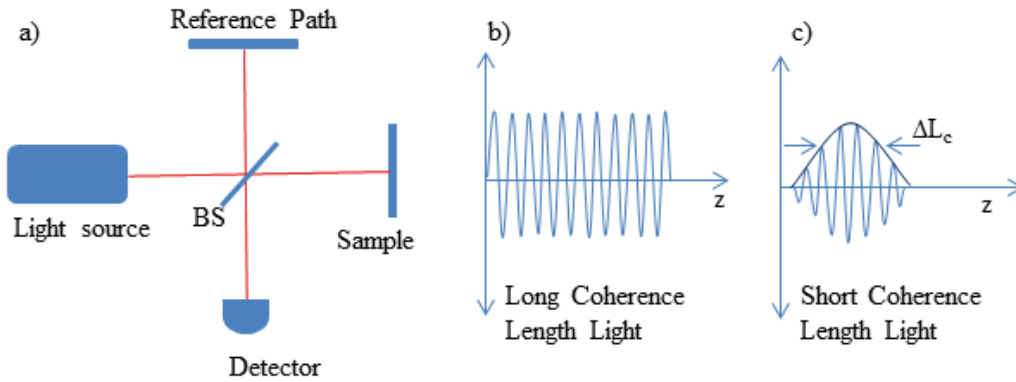
Figure 2.1: a) Heart of OCT system is Michelson type interferometer. b) Long coherence light source. c) Short coherence light source

In the laser light source interference will happen even if the path length varies as long as the difference of distance travelled by two light beams is within coherence length (Lc) of source which is in meters. However, if short pulses of light or low coherence light source are used, interference will occur only if path length of the reference beam and backscattered beam from sample is within coherence length of light. As the coherence length is small (in micrometers), signal intensity decreases sharply with mismatch in path length and so longitudinal/axial information at particular location of sample can be determined with high resolution. To get the actual depth information in sample, the optical delay is divided by group velocity index of the tissue, as the velocity of light is slower in tissue compared to air. Depth of imaging in OCT is limited by optical absorption and optical attenuation by tissue/material. Long wavelength light source can be used for deeper imaging, as penetration depth of infrared light in tissue increases with wavelength.

Axial resolution in OCT imaging depends upon coherence length of light source. Unlike other microscopy techniques, in which large aperture gives better resolution, OCT can have high resolution with small aperture. This feature is particularly exploited in deep tissue imaging. The longitudinal resolution considering a Gaussian source line shape is given by:

$$\Delta z = \frac{2\ln(2)}{\pi} \frac{\lambda^2}{\Delta\lambda} \qquad \text{...Equation 2.1}$$

where, Δz and $\Delta\lambda$ are the full widths at half maximum of the autocorrelation function and power spectrum respectively and λ is the central source wavelength. The transverse resolution depends upon the beam width inside sample similar to conventional microscopy. The transverse resolution is given by:

$$\Delta x = \frac{4\lambda}{\pi} \frac{f}{d} \qquad \text{...Equation 2.2}$$

where d is the spot size on objective lens and f is the focal length.

Also, relation of transverse resolution with depth of focus or confocal parameter b is given by:

$$b = \frac{\pi \Delta x^2}{2\lambda}$$ ...Equation 2.3

Hence, similar to conventional microscopy, depth of focus decreases with increase in transverse resolution (decrease in Δx).

Signal to noise ratio in OCT can be calculated using standard techniques from optical communication and is given by:

$$SNR = 10 \log \left\{ \frac{\eta P}{2h\nu NEB} \right\}$$ ...Equation 2.4

where P is detected power, NEB is noise equivalent bandwidth of the detection, hν is the photon energy and η is the detector quantum efficiency.

OCT performs multiple axial scans laterally to form a two dimensional image or a B scan as shown in Figure 2.2. Several B scans are combined to generate a three dimensional view of sample.
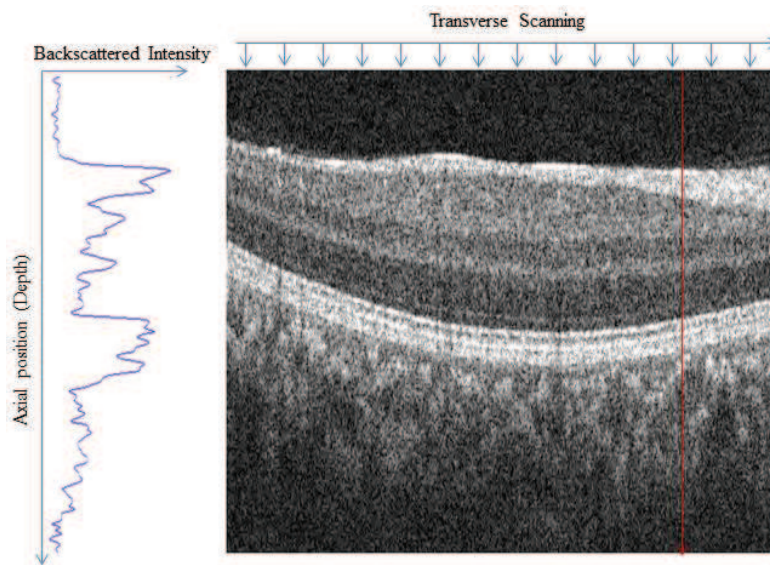
Figure 2.2: Each A-scan contains the depth information of backscattered light at a single point on sample surface. Multiple A-scans along transverse direction, are combined to form a cross sectional image or B scan along a line on sample surface

2.4   Types of OCT

2.4.1   Time Domain Optical Coherence Tomography (TD-OCT)

Previous OCT systems were based on time domain detection. Schematic of TD-OCT is shown in Figure 2.3. In Michelson interferometer, light from a low coherence light source is split in two arms of interferometer: sample arm and reference arm. In sample arm, light beam is directed and scanned on sample to be imaged. Reference arm contains a mechanical scanner to vary the optical path length. Backscattered light from sample arm is interfered

with that of light from reference arm. Only when the optical path length of two arms is within coherence length of light source, interference will be constructive and provide high intensity signal, otherwise signal intensity will diminish. At each point on sample surface being imaged, photo-detector records multiple times at different locations along depth axis by varying the path length in reference arm. This is termed as 'A-scan'. Galvanometer optical scanners in sample arm scans multiple points or number of A-scan in transverse axis to form two dimensional cross sectional image, termed as a 'B scan'.

The axial resolution depends inversely on coherence length of light source. Also, coherence length varies inversely with bandwidth of light source. Therefore broad band laser or super luminescent diode (SLD) is used as light source. SLD has short coherence length. Time domain OCT system has resolution about 10 microns. The low acquisition rate causes motion artifacts due to eye movement, but increase in acquisition speed will degrade image resolution. TD-OCT can produce a B scan, with 400 A-scans per second and resolution 1024 points in 6mm of tissue, in 1.6 seconds.
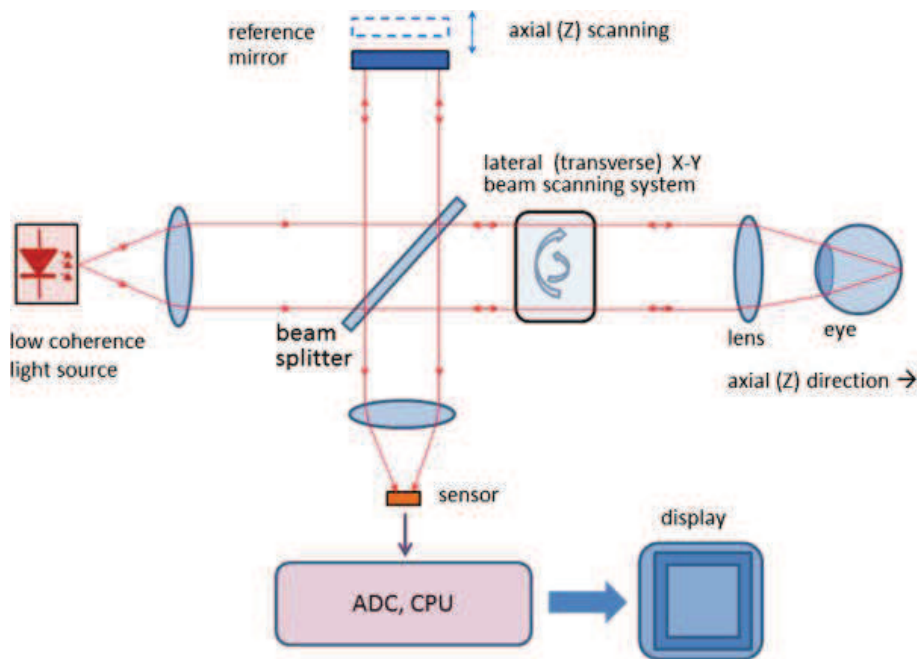
Figure 2.3: Time domain OCT using low coherence light source and an interferometer with scanning reference arm

2.4.2 Fourier Domain Optical Coherence Tomography (FD-OCT)

2.4.2.1. Spectral Domain / Fourier Domain Optical Coherence Tomography (SD/FD-OCT)

Spectral domain/ Fourier domain OCT uses a spectrometer with a line scan camera in detection arm and broadband light source to detect echo time delay of light. Figure 2.4 shows the schematic of Spectral / Fourier domain OCT. A broad band light source is

coupled in Michelson interferometer, with a reference arm and sample arm. The backscattered light from sample is made to interfere with light from reference arm. This interference is detected using a spectrometer and a line scan camera. Different time delays of light generate different frequency of fringes in the interference pattern. More delay results in higher oscillation frequency in interference spectrum. Fourier transform of the interference pattern provides the magnitude and delay of backscattered light.

Simultaneous recording of backscattered light greatly improves the sensitivity in Spectral / Fourier domain OCT [7-9]. Axial resolution depends upon the coherence length of light source. The transverse resolution depends upon the beam width on sample. The high imaging speed in Spectral / Fourier domain OCT sharply reduces the motion artifacts due to eye movement. Fast scanning allows real time three dimensional (3D) imaging, generating volumetric dataset for better visualization of tissue structures. In Fourier domain OCT, access to interference spectrum enabled a wide range of phase sensitive applications such as Doppler imaging of blood flow [10-14]. Also, Fourier domain OCT supports broad bandwidths and enables ultrahigh axial imaging speed [15].
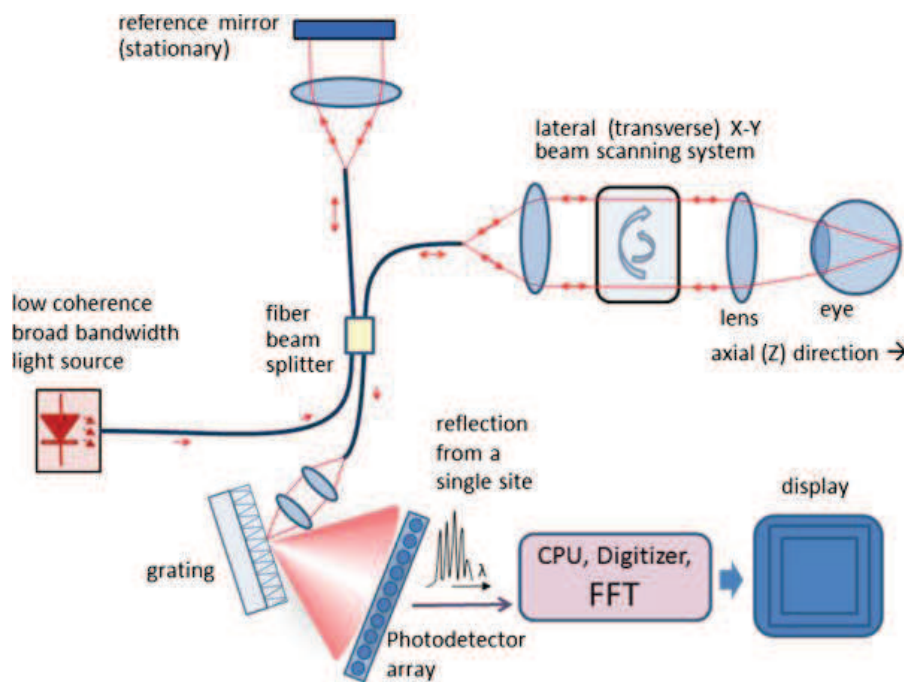
Figure 2.4: Schematic of SD OCT system

2.4.2.2. Swept Source / Fourier Domain Optical Coherence Tomography (SS/FD-OCT)

Swept source / Fourier domain OCT is a different approach to spectrum / Fourier domain OCT. Figure 2.5 shows the schematic of Swept source / Fourier domain OCT. In SS/FD-OCT intensity data is recorded simultaneously using a broadband light source and a spectrometer. But in swept source OCT, a tunable laser source and single photo-detector is

used for recording at different wavelengths. Beat frequencies in interference signal are generated by optical delay, which are detected. Fourier transform of detected signal provides optical delay information. Swept source / Fourier domain OCT systems have advantages of sensitivity, high imaging speed and high resolution [7].

Swept source / Fourier domain OCT uses high speed detectors, unlike spectral / Fourier domain OCT system which employs line scan camera. Swept source / Fourier domain OCT system can use long wavelength light source, for which line scan camera may not be available and reduce the cost of system by replacing relatively expensive line scan cameras at longer wavelength. Moreover, long wavelength light has advantage of deep penetration in high scattering tissue. Spectrometer loss of light and alignment problems are also eliminated in swept source / Fourier domain OCT and system became more compact.

In a swept source OCT system, the laser line-width decides the frequency resolution and resolution can be better than a spectrometer based spectral domain / Fourier domain OCT system. This enables imaging at greater depth range and higher number of axial pixels compared to spectral / Fourier domain OCT. In swept source OCT, the absence of fringe wash out problems which occur with rapid beam scanning in spectrometer based detection, allows rapid imaging of larger fields of view than spectral / Fourier domain OCT.
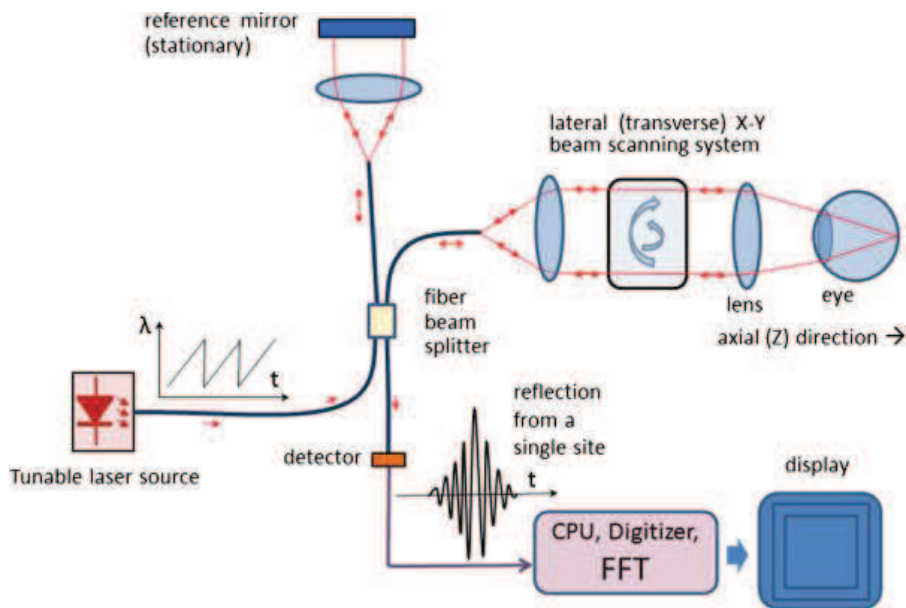
Figure 2.5: A Swept source / Fourier domain OCT system

2.5   Applications of OCT

OCT imaging provides high resolution, cross-sectional and three dimensional images of biological tissue or material in real time without excision or preprocessing, which make it very useful and attractive imaging technology in biomedical engineering and industry. OCT

11

is now an essential tool for diagnosis of retinal diseases and glaucoma. OCT retinal images provides high resolution structural information, indicating thickness changes, tissue degeneration or generation, lesion, blood clotting/ vascular obstruction, RPE detachment, change in optical property, scattering and opacity etc. Also, progress in treatment can be easily monitored.

With the use of optical fibers, OCT can easily be integrated with wide variety of instruments such as catheter, needle, small endoscope, ophthalmoscope, probes or any other surgical instruments. OCT is an emerging technology for intravascular imaging, where it can identify unstable plaques that are prone to rupture, producing myocardial infarction [4].

2.6   Image Segmentation

Image Segmentation can be defined as the partitioning of an image into meaningful/useful regions that have strong correlation with objects or areas of the real world contained in the image. Image segmentation of retinal OCT images is performed in order to localize intra-retinal boundaries. The thickness of various layers provides critical information for diagnosis and study of macular diseases. Automatic image segmentation is necessary step for quick analysis of macular structure and their thickness evaluation. The main challenge in OCT image segmentation is to design a system which functions properly in clinical environment. In diseased conditions macular structures can be highly altered. Moreover OCT images have intrinsic speckle noise and low signal-to-noise ratio. This makes image segmentation even more challenging. No segmentation method can be expected to perform equally in all cases.

With advances in OCT imaging, multiple frames at high imaging speed are being acquired. For its complete exploitation, automated three-dimensional segmentation algorithms are necessary.

2.7   Literature Survey

Different segmentation approaches have been introduced for retinal OCT image segmentation. They can be classified into intensity-based; gradient-based, active contour-based and based on graph theory. The segmentation algorithms are designed to work on A-scan, B-scan / cross-sectional image or three-dimensional data cube.

F. Tapio et al presented a segmentation technique based on signal intensity variation for two layers ILM and RPE [16].   Qi Yang et al performed two step segmentation; using gradient information in dual scale, using local and complimentary global gradient information along with shortest path search for edge detection. Nine retinal boundaries were successfully obtained in healthy retinal scans [17]. Xusheng Zhang et al demonstrated automated retinal

layer segmentation in FD-OCT images using search strategy based on locally weighted gradient extrema, coupled with an error removing technique based on statistical error estimation. Seven intra-retinal layers were segmented [18].

Y. Azadeh et al performed OCT image segmentation using Chan-Vese's energy minimizing active contour without edges and circular prior shape model, on retinal OCT images of rat [19]. Akshaya Mishra et al showed segmentation based on active contour on retinal images from healthy and diseased rodent models. Two step kernel based optimization scheme, first identify approximate location of each layer and then refine each layer [20].

Milan Sonka et al used a graph theory based approach with ability incorporate regional information and varying feasibility constrains [21]. Pascal A. Dufour et al performed graph based segmentation that uses soft constrain to add prior information from learned models [22]. Stephanie J. Chiu et al presented an automated approach for segmentation of retinal images using graph theory and dynamic programming. And accurately segmented eight retinal layer boundaries in retinal images obtained from healthy adult eyes [23]. They further used it for segmentation of AMD pathology in clinical trial [24].

K. A. Vermeer et al showed an automated segmentation by classifying each pixel in retinal layers. For each layer, simple feature were defined and machine learning classifiers were trained based on manually labeled examples [25].

Chapter 3
Human Eye

3.1 Anatomy of Human Eye

Eye is the light sense organ. The anatomy of human eye is shown in Figure 3.1. The diameter of adult human eye is about 24 mm, but it is not a perfect sphere. Light enters into eye through iris and pupil. Iris - color of eye, controls amount of light entering eye. Light beam is focused on fovea by cornea and lens. Fovea is the most sensitive region and sharpest vision spot of macula. Transparent fibers holding lens adjusts focal point of lens and enable focusing vision at nearer or far object.
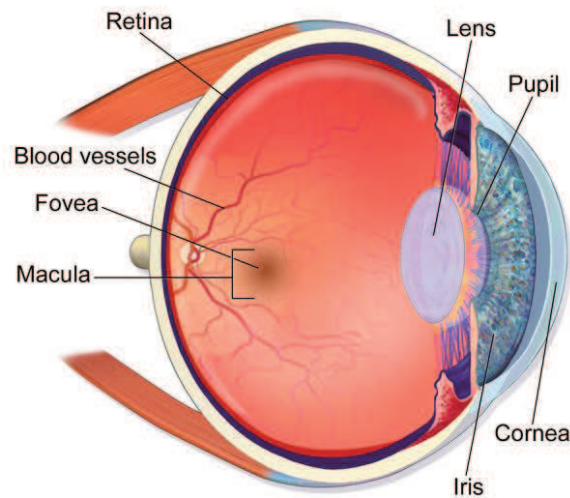
Figure 3.1: The human eye

Retina is about 0.5 mm thick inner layer in back of eye. A retinal image as seen in ophthalmoscope is shown in Figure 3.2. The circular to oval area measuring 2×1.5 mm in center of retina is optic nerve center. Major blood vessels of retina radiates through optic nerve center. The slightly oval shaped, blood vessel free reddish spot is fovea and is the center of macula.

Retina consists of several layers of interconnected neurons. Light sensitive cells or photoreceptor cells of retina are rods and cones. Rods provide black and white vision and works in dim light conditions. Cons perceive color information and works in bright light conditions. These photoreceptor cells are in back side of retina. Ganglion cells, which transport signal to brain lies in front side nearer to lens. Therefore light has to penetrate these layers before reaching photoreceptor cells, i.e. rods and cons. Light photons generate neural signals in photoreceptor cells i.e. rods and cons, which are further processed and in turn generates electrical signal in form of action potential. The electrical signal is then transmitted to optic disk and along optic nerve to brain. Retinal nerve fiber layer is the axons of ganglion cells and is called Helen fibers in the vicinity of fovea. Eye is filled with thick transparent fluid, called vitreous humor.
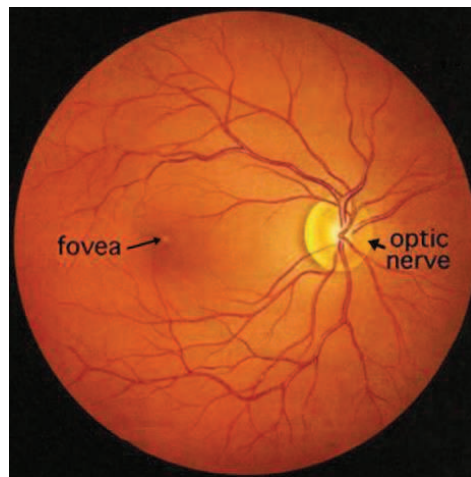
Figure 3.2: Retinal image as seen through ophthalmoscope[27]

Macula is an oval-shaped highly pigmented yellow spot near the center of the retina of the human eye. It has a diameter of around 6 mm. Macula is a specialized region for high acuity vision. Fovea lies at the center of macula and has diameter about 200 micro meters. Fovea size is relatively small compared to the rest of retina, but the fovea is the only area of the retina where 20/20 vision is attainable, and very important for seeing fine detail and color. At fovea, cons are highly concentrated and the ratio of ganglion cell to photoreceptor is about 2.5, i.e. each cone cell is connected to 1 to 3 ganglion cells [26]. At the fovea pit, other retinal layers are displaced leaving thinnest layer of retina consisting ganglion cells and cone cells. The complete layering of the retina then appears gradually along the fovea slope until the rim of the fovea is made up of the displaced second and third-order neurons related to the central cones. Here the ganglion cells are piled into six layers so making this area, called the foveal rim or parafovea, the thickest portion of the entire retina. Figure 3.3 shows the thickness variation in macula near fovea.
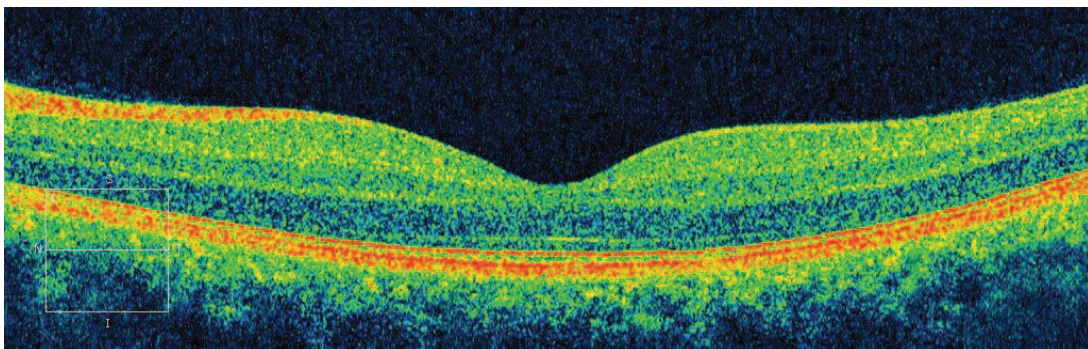
Figure 3.3: OCT image of healthy retina

16

3.2   Retinal Layers

A light micrograph of a vertical section through central human retina is displayed in Figure 3.4.
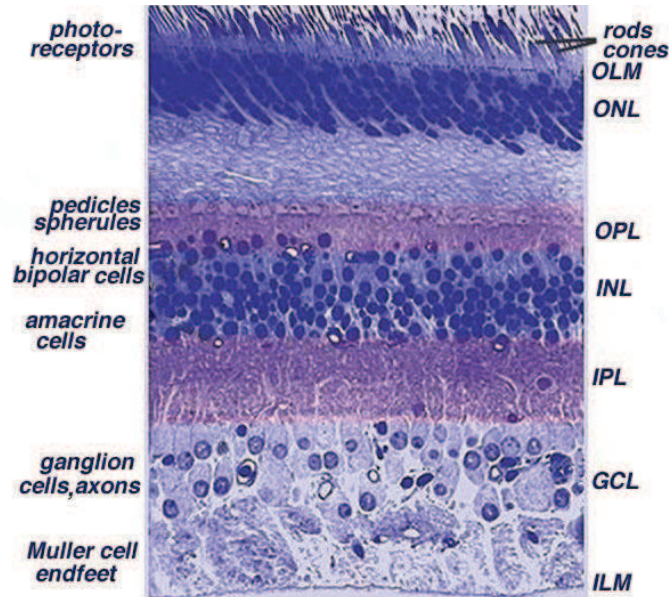
Figure 3.4: Light micrograph of a vertical section through central human retina[27]

Various layers in retina from vitreous (front) to choroid region (back) are:

1. Inner limiting membrane: ILM is the inner surface of retina surrounding vitreous humor. It is composed of laterally contacting Muller cell end feet and associated basement membrane constituents. It acts as diffusion barrier between vitreous humor and nerve fibers.

2. Nerve fiber layer – consists of axons of the ganglion cell nuclei. They act as transmission lines to brains.

3. Ganglion cell layer – contains nuclei of ganglion cells, the axons of which become the optic nerve fibers for messages transmission.

4. Inner plexiform layer – IPL is neuropil area, which function as a relay station for the vertical-information-carrying nerve cells, the bipolar cells, to connect to ganglion cells. Here, horizontally- and vertically-directed amacrine cells interact in further networks to influence and integrate the ganglion cell signals. This neural processing in the inner plexiform layer generates the message containing the visual image, which is transmitted to the brain along the optic nerve.

5. Inner nuclear layer – contains the nuclei and surrounding cell bodies (perikarya) of the amacrine cells, bipolar cells and horizontal cells. INL is thicker in central area compared to peripheral area of retina, because of dense cone connecting second

17

order neuron (cone bipolar cells), and closely spaced horizontal cells and amacrine cells concerned with cone pathways.

6. Outer plexiform layer – OPL is the area of neuropil, where connections between rod and cones, and vertically running bipolar cells and horizontally oriented horizontal cells occur. Here, projections of rods and cones ending in the rod spherule and cone pedicle, respectively. These make synapses with dendrites of bipolar cells.

7. Outer nuclear layer – is composed of cell bodies of rods and cones. It has nearly same thickness in central and peripheral retina, but cons are more concentrated at fovea.

8. External limiting membrane – layer that separates the inner segment portions of the photoreceptors from their cell nucleus

9. Photoreceptor layer – rods/cones.

10. Retinal pigment epithelium - single layer of cuboidal cells.

3.3 Pathology of Retina

3.3.1 Macular degeneration

Age related macular degeneration (AMD) is a medical condition that usually affects older adults and results in a loss of vision in the center of the visual field (the macula) because of damage to the retina. In the dry (nonexudative) form, cellular debris called drusen accumulates between the retina and the choroid, and the retina can be detached. In the wet (exudative) form, which is more severe, blood vessels grow up from the choroid behind the retina, and the retina can also be detached. It can be treated with laser coagulation, and with medication that stops and sometimes reverses the growth of blood vessels [28]. A macular OCT image of wet-AMD patient is shown in fig. 3.5.
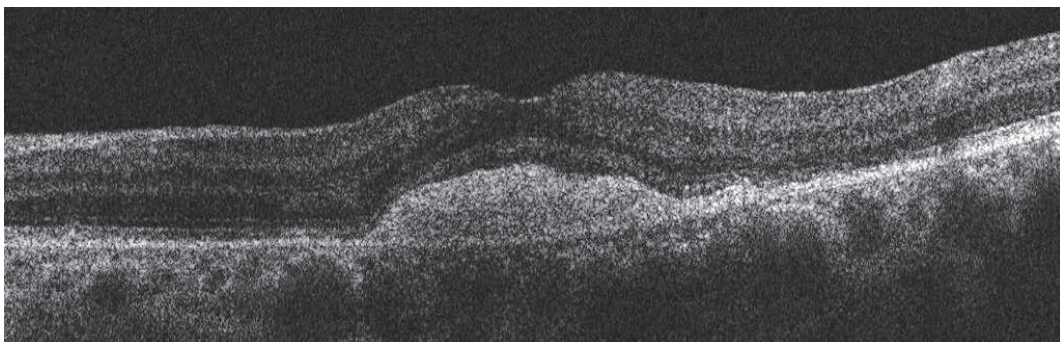
Figure 3.5: A macular OCT image of a wet-AMD patient

3.3.2 Diabetic Retinopathy

Diabetic retinopathy is damage to the retina caused by complications of diabetes, which can eventually lead to blindness. It is an ocular manifestation of diabetes, a systemic disease,

which affects up to 80 percent of all patients who have had diabetes for 10 years or more. Macular edema is main reason of reduced vision in nonproliferative diabetic retinopathy. The edema starts with focal edema, progresses to diffuse edema, and then may become cystic. Serous detachment is part of progress of diabetic edema.

As the disease progresses, severe nonproliferative diabetic retinopathy enters an advanced proliferative (PDR) stage when blood vessels proliferate. The lack of oxygen in the retina causes fragile, new, blood vessels to grow along the retina and in vitreous humor. Without timely treatment, these new blood vessels can bleed, cloud vision, and destroy the retina.

3.3.3 Vascular Occlusion of Retina

Vascular occlusion is a blockage of a blood vessel. Retinal arterial occlusion leads to rapid death of retinal cells, thereby resulting in severe loss of vision. When an occlusion of central retinal artery is observed after a few hours, retinal edema is seen as cherry-red central stain on examination. Optical coherence tomography performed in first few days allows seeing marked edema, localized in the internal layers: the NFL, the ganglion layer, the internal plexiform layer and the INL of the bipolar cells. An increased reflectivity and thickness of INL and the RNFL can be observed [29].

3.3.4 Retinal Epitheliopathy

Central serous chorioretinopathy (CSCR) most commonly occurs in men between age 25 and 45. It is often bilateral and recurrent. In serous RPE detachments, multiple points of diffusion may be visible where the RPE is detached from Bruch's membrane, forming liquid filled spaces.

Chronic epitheliopathy usually occurs in people 45 to 69 years of age. It is associated with points of diffusion, dystrophic changes of the RPE and serous RPE detachments. Areas of RPE may be absent and areas of gravitational epitheliopathy can be observed. Choroid neovascularization is common.

3.4 Glaucoma

Glaucoma is a term describing a group of ocular disorders with multi-factorial etiology united by a clinically characteristic intraocular pressure-associated optic neuropathy. It is not a single entity and is sometimes referred to in the plural as the glaucomas. All forms are potentially progressive and can lead to blindness. The diverse conditions that comprise glaucoma are united by a clinically characteristic optic neuropathy: glaucomatous optic neuropathy (GON). Evidence suggests that the primary site of neurological injury is at the optic nerve head [29].

3.5   Retinal OCT Images

Optical coherence tomography (OCT) is now a standard tool for in vivo noninvasive, noncontact analysis of retinal tissue for diagnosis and management of retinal diseases and glaucoma. The high resolution of SD-OCT nearly 5 microns provides detailed retinal structural information. Fast speed 27,000 A-scans per second in SD-OCT makes three dimensional (3-D) imaging practical in clinical environment. It takes about 2.4 seconds to scan a macular cube of 512×128. These OCT retinal scans are highly reproducible.

Optical coherence tomography allows clinical observation, measurement and identification of structures that are otherwise not easily visible, such as external limiting membrane (ELM) and the junction between the internal and external segment of photoreceptors (IS/OS junction). It also shows various types of lesions with altered morphology, altered reflectivity, and optical blank areas. OCT performs the following function: [1]

- o   Measures retinal thickness
- o   Measures the retinal nerve fiber layer (RNFL)
- o   Measures the volume of retina
- o   Creates retinal thickness maps
- o   Measures various parameters of optic disc
- o   Displays three-dimensional views
- o   Provides classic C-scan (en face) analysis, creates horizontal tissue sections
- o   Isolates and creates maps of internal limiting membrane (ILM) and the retinal pigment epithelium (RPE)

3.5.1 Two Dimensional OCT Image

B scan image of a healthy human eye is shown in Figure 3.6. Various layers of retina are marked on image.
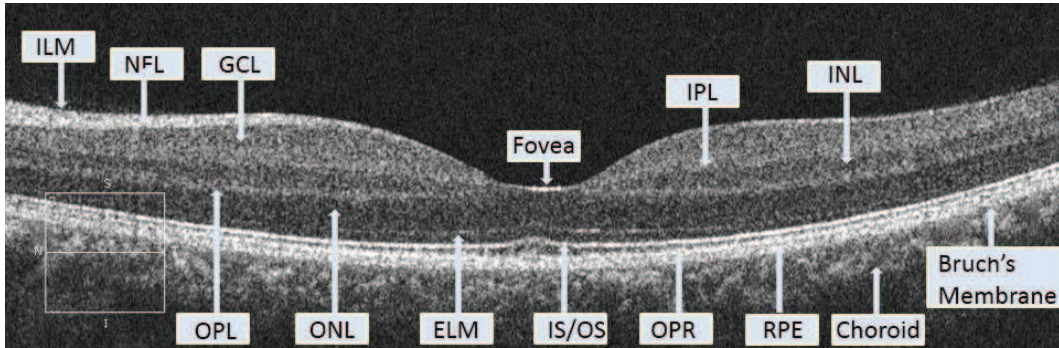
Figure 3.6: OCT retinal scan of a healthy human eye. Various layers of retina are marked

3.5.2 Three Dimensional OCT Image

Multiple B scans or cross-sectional images are combined to form a 3 dimensional image as shown in fig. 3.7.
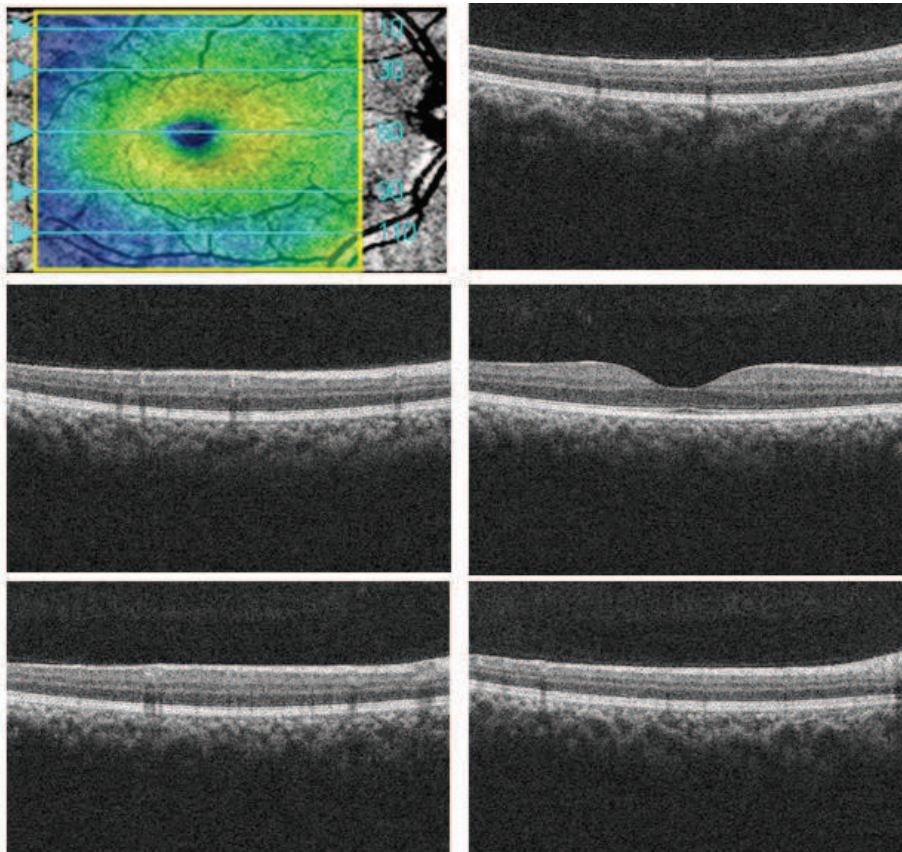
Figure 3.7: Multiple macular OCT scans are performed to make a 3-D view

Figure 3.8 shows a three-dimensional view of OCT retinal scan of a healthy volunteer.
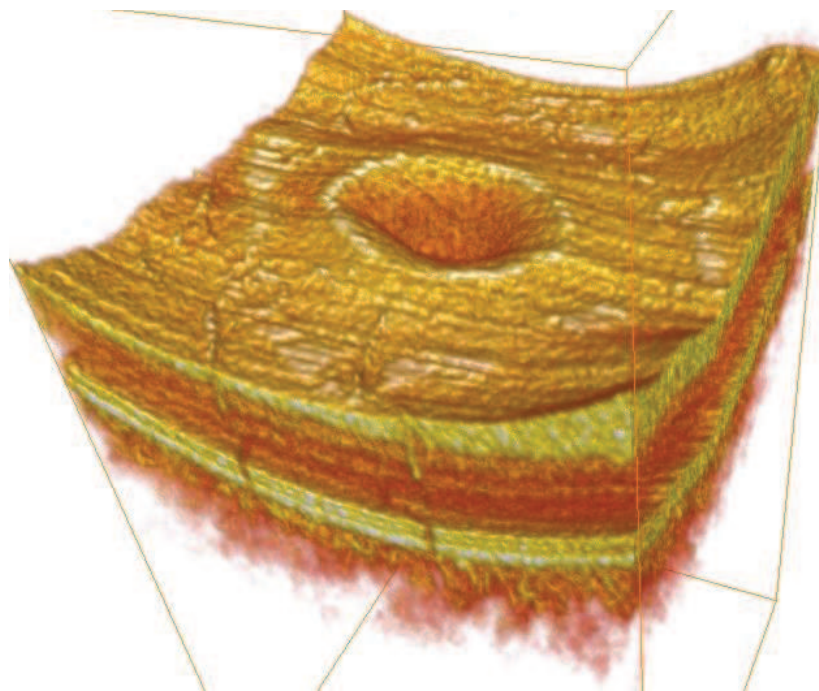
Figure 3.8: A three-dimensional view of OCT retinal scan of a healthy volunteer

3.5.3 Clinical OCT Report

Figure 3.9 shows clinical OCT report of a healthy volunteer. In this report, RPE-ILM thickness plot is shown. RPE and ILM are the two extreme of macula. The volume of macula cube is 10.4 mm3. The cube average thickness is 291μm.

Name: **Chakole, Ashish**

ID: CZMI1279723294
DOB: 7/27/1989
Gender: Male
Technician: Operator, Cirrus

Exam Date: 10/24/2013
Exam Time: 10:14 AM
Serial Number: 400-12294
Signal Strength: 9/10

CZMI

ZEISS

Macula Thickness : Macular Cube 512x128   OD ● ○ OS

Overlay: ILM - RPE Transparency: 50 %

ILM-RPE Thickness (μm)

Fovea: 274, 65

ILM - RPE

ILM

RPE
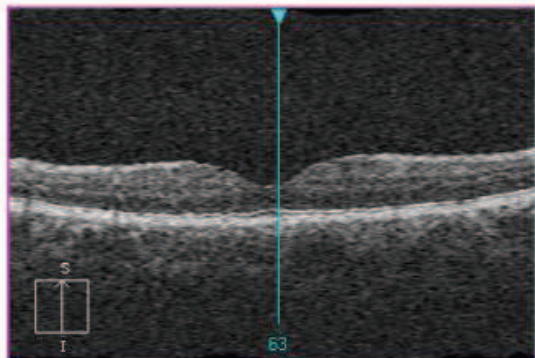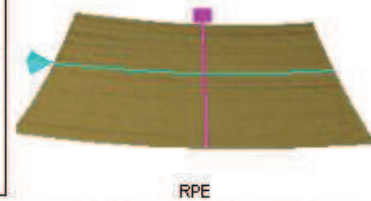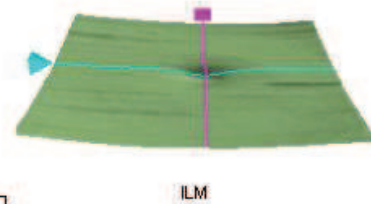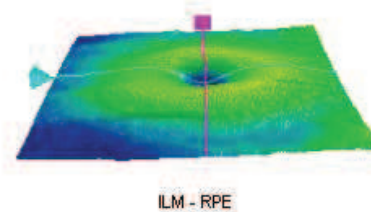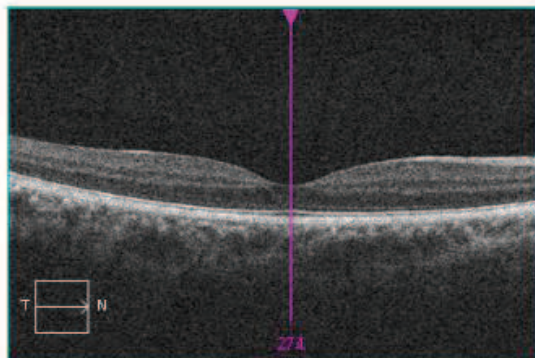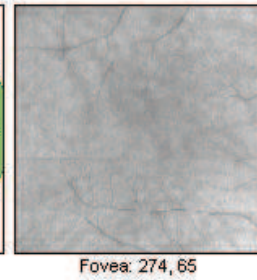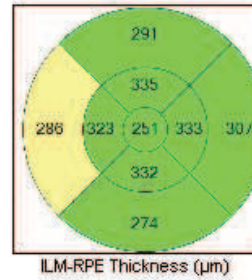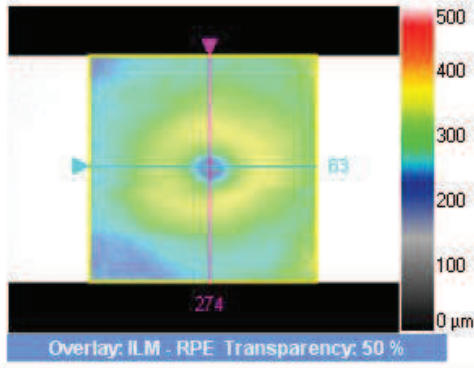
Diversified: Distribution of Normals

- 99%
- 95%
- 5%
- 1%

⚠	Central Subfield Thickness (μm)	Cube Volume (mm³)	Cube Average Thickness (μm)
ILM - RPE	251	10.4	291

Comments

Analysis Edited: 6/26/2014 4:23 PM

Doctor's Signature

SW Ver. 6.5.0.772
Copyright 2012
Carl Zeiss Meditec, Inc
All Rights Reserved

Page 1 of 1

Figure 3.9: A machine generated clinical OCT report

Chapter 4
Experiments and Results

4.1 Experimental Setup

The macular OCT images of healthy volunteers were obtained using Citrus HD-OCT system. Each three dimensional scan covers macular volume of 2mm×6mm× 6mm and provides data of dimension 1024×512×128. At this specification, OCT System takes about 1.6 second to take one three dimensional scan. The axial resolution of OCT system is 2μm. The transverse resolution i.e. between two A-scans is about 12μm[30].

The segmentation algorithm was implemented on MATLAB (The MathWork, Inc). Program runs on a personal computer (64-bit OS, Intel(R) Core(TM) i5-2400 CPU@3.10GHz, 4GB RAM).
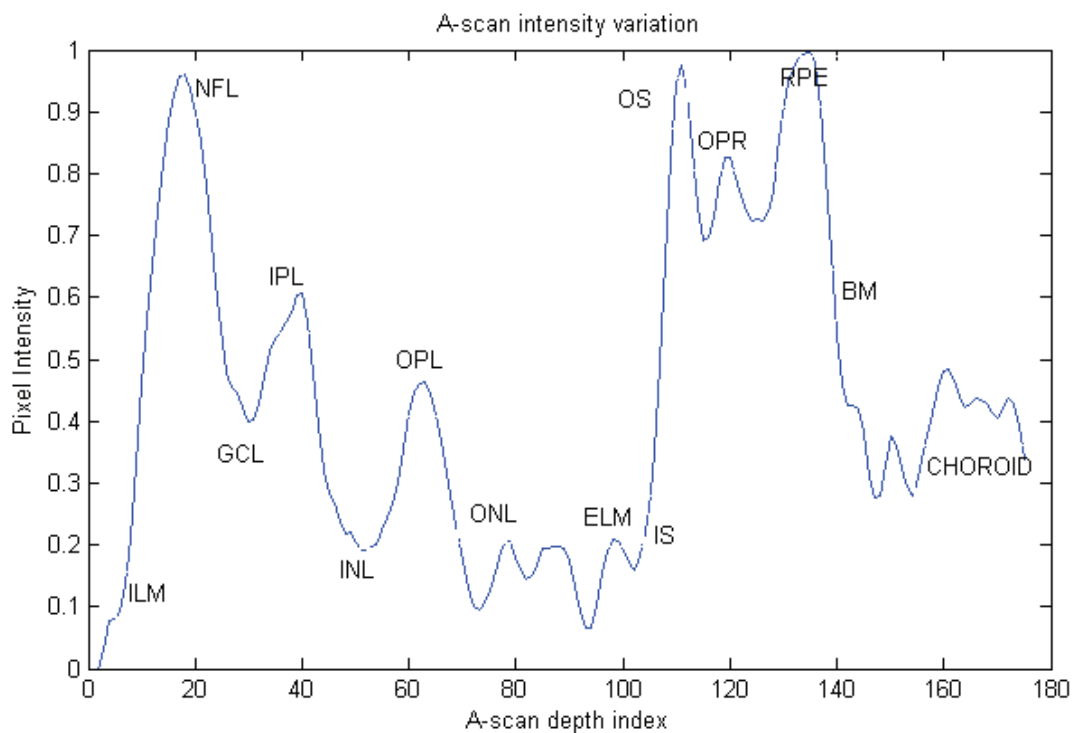
Figure 4.1: Intensity profile of A-scan used for marking various layers/boundaries.

4.2 Two Dimensional Image Segmentation of Retinal OCT Image using Gradient Method

The macular OCT image segmentation algorithm employed gradient information to detect layer boundaries. In this algorithm, the axial gradient information was used to mark various macular layer boundaries in macular OCT images. The intensity variation in A-scan is similar for all A-scans, except for those at fovea region. The change in intensity along A-scan has a unique pattern. For example, vitreous to NFL boundary and IS/OS junction are the two points of highest intensity rise. Similarly Bruch's membrane, NFL-GCL and OPL-ONL has sharp intensity drop. Figure 4.1 shows the typical intensity profile of A-scan used

25

for segmentation. Along with the axial gradient, location of various boundaries and the change in intensity i.e. bright to dark or dark to bright; too were used to mark layer boundaries. Macular layers were obtained in each B-scan individually. Thus obtained macular layers were smoothened using a modified median filter. Figure 4.2 shows the flow chart of gradient based segmentation process.
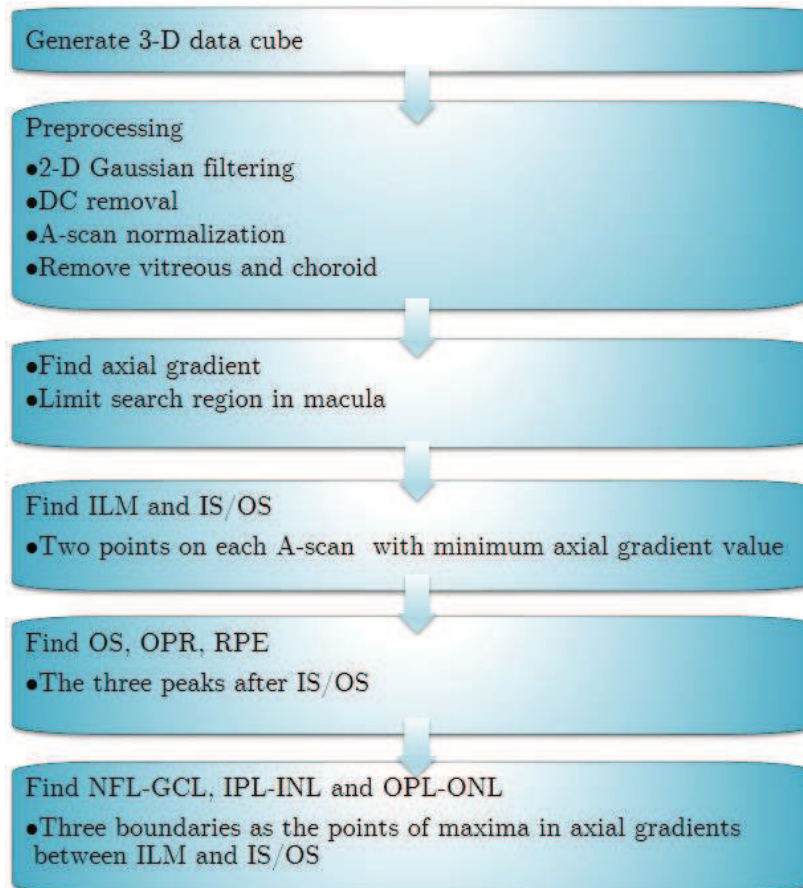
Figure 4.2: Flow chart of gradient based segmentation method

4.2.1   Denoising and Finding Area of Interest

All the 128 macular OCT images (1024×512) obtained from a macular cube scan were combined in a form of 3-D matrix (1024×512×128). Image preprocessing was performed in three steps: 1) 2-D Gaussian filtering, 2) removing dc component in each A-scan, and 3) normalization of each A-scan. Denoising was performed in order to remove speckle noise and smoothen the intensity variation of image. A Gaussian filter of size 5×7 and SD 2 was used for denoising. The dc component in each A-scan was removed and A-scans were normalized. Each A-scan Vitreous and choroid region occupies most of space in macular OCT images. The processing time and volume of data to be processed, was minimized by identifying the region of interest. Two boundaries: anterior and posterior, just before ILM

and after Bruch Membrane were obtained. To detect anterior boundary, we used binary image with threshold 0.2. The first white pixel in each A-scan of binary image was marked as anterior boundary. Similarly posterior boundary was obtained from binary image with threshold 0.4, but scanning for first white pixel was performed in reverse direction i.e. from choroid side. The rows of image, above minimum of anterior boundary and below maximum of posterior boundary, were removed in order to minimize image data for further processing. The data cube dimension was reduced to nearly (400×512×128) from actual (1024×512×128) after removing the vitreous and choroid region. Figure 4.3(a) shows the OCT image near fovea region after removal of vitreous and choroid region and (b) after preprocessing.

4.2.2 ILM and IS/OS detection

The ILM and IS/OS boundaries show highest gradient i.e. intensity variation along A-scan. Axial gradient was obtained using matrix of size [7×1] with values [1; 1; 1; 0; -1; -1; -1]. Figure 4.3c) shows the axial gradient B-scan near fovea. This provided gradient in each A-scan in larger area. Thus obtained axial gradient was used for detection of all boundaries. ILM and IS/OS are the two points of minimum value in axial gradient matrix in each A-scan. First, two points in each A-scan with minimum value in axial gradient matrix and at least 40 pixels apart were detected. The point nearer to the anterior boundary was marked as ILM and point nearer to the posterior boundary was marked as IS/OS. ILM and IS/OS were smoothened with a modified median filter. Figure 4.3d) shows the ILM and IS/OS layers overlapped on actual B-scan.
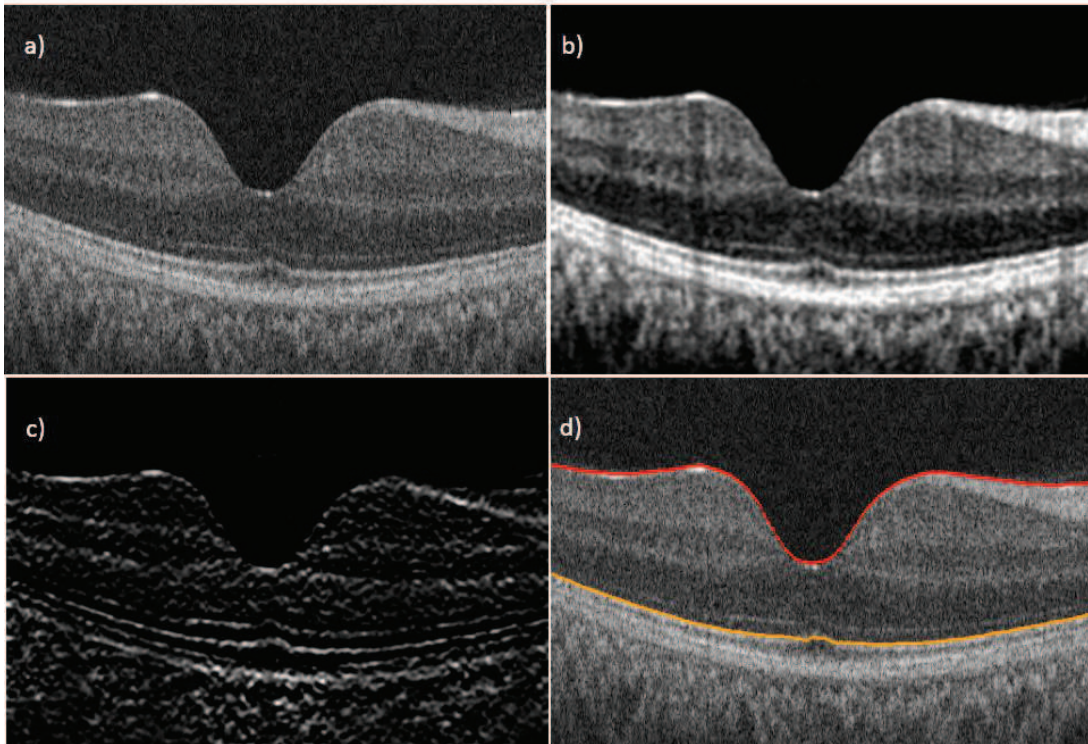
Figure 4.3: a) OCT image near fovea. b) Image after preprocessing. c) Axial gradient of image. d) ILM (red) and IS/OS (yellow) overlapped on image

4.2.3 RPE Detection

The RPE layer shows the highest intensity in backscattered light. Blood shows higher scattering for infrared light compared to surrounding macular tissue. The blood vessel on macula scatters most of light falling on it, which in turn creates shadow in OCT image and information behind blood vessel is lost. And so, locating RPE as the point of highest intensity in each A-scan fails due to blood vessels and needs error correction mechanism [18]. With the knowledge of IS/OS, macula was divided into two regions: between ILM and IS/OS, and below IS/OS.

To mark RPE, three peaks between IS/OS and posterior boundary were obtained using a peak finder. The three peaks from IS/OS were marked as OS, OPR and RPE respectively. A modified median filter was used to smooth layer boundaries. Figure 4.4 shows the 3-D view of ILM and RPE.
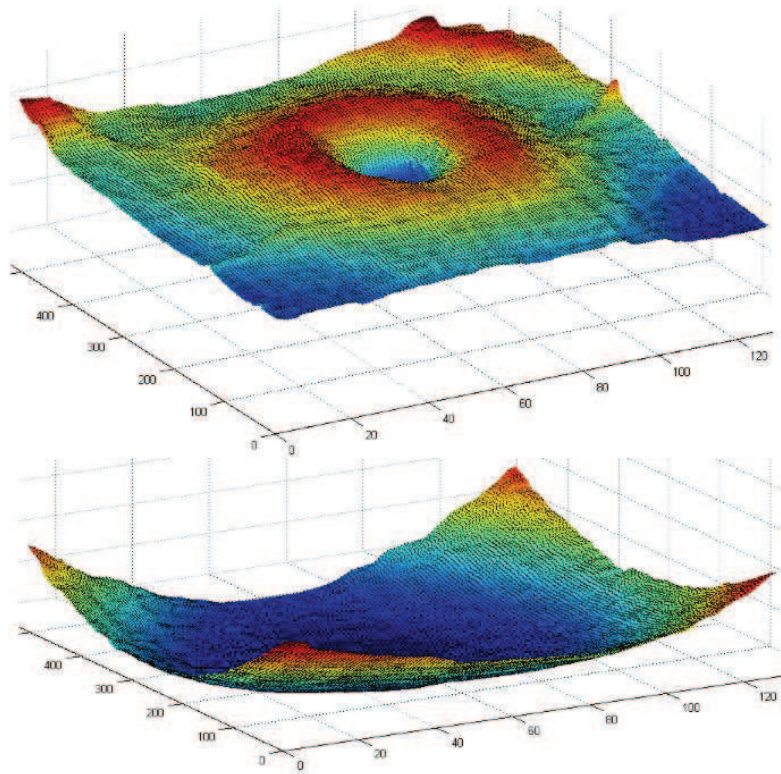
Figure 4.4: Shows the 3-D plot of ILM and RPE

4.2.4　Finding Other Layer Boundaries

In between ILM and IS/OS, NFL-GCL, IPL-INL and OPL-ONL boundaries have bright to dark transition. In the axial gradient matrix, bright to dark transition shows in positive maxima. Three points of maxima in axial gradient between ILM and IS/OS were obtained. The point of maxima nearer to IS/OS were marked as OPL-ONL boundary. Again, two maxima points in axial gradient were obtained between ILM and OPL-ONL. The maxima point nearer to ILM was marked as NFL-GCL boundary. IPL-INL boundary was marked as the point of maxima in axial gradient between NFL-GCL and OPL-ONL boundaries. All layers were smoothened using a modified median filter of size 10×10. Figure 4.5 shows the segmented layers/boundaries marked on OCT images at various position on macula.
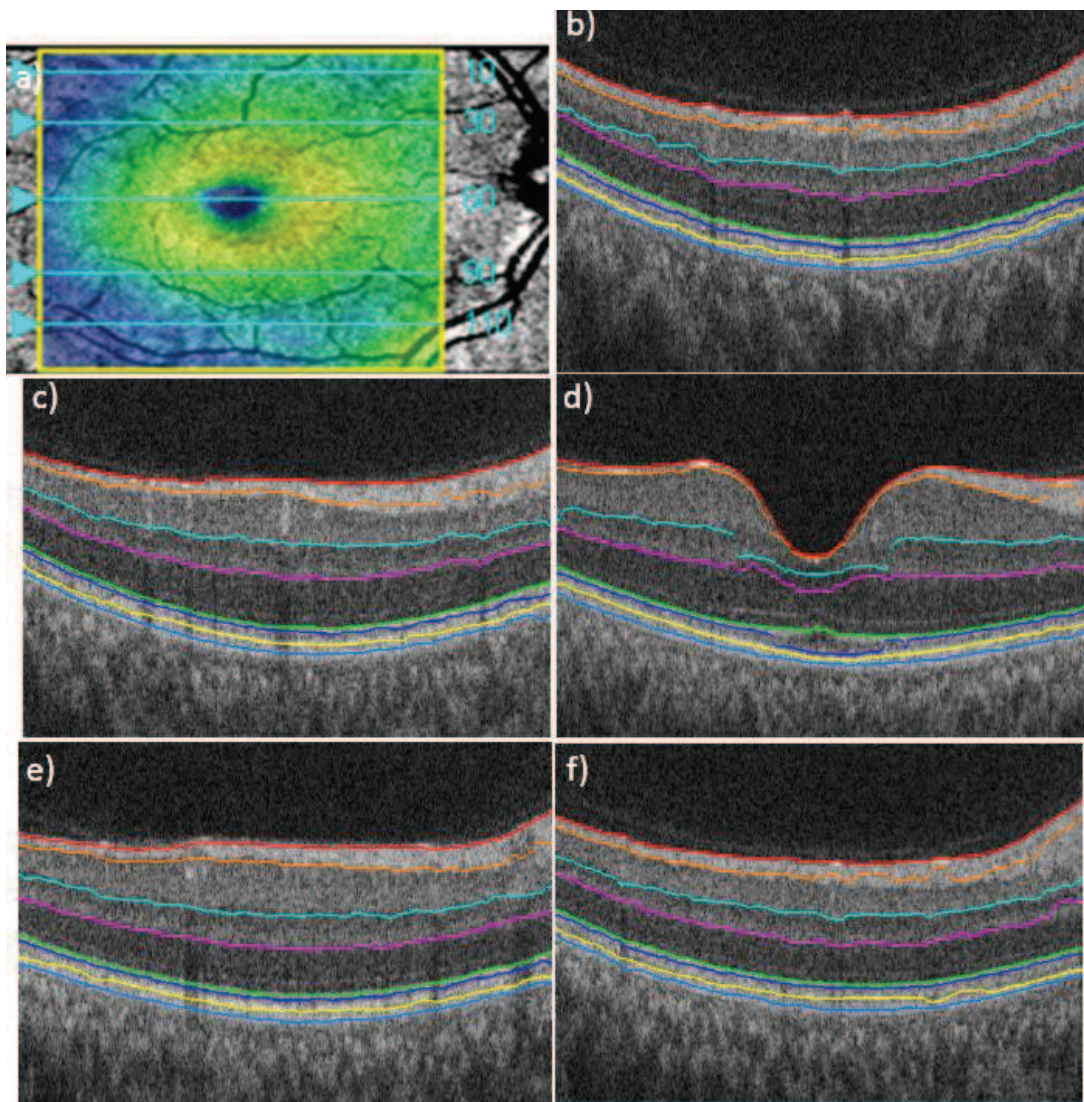
Figure 4.5: shows the segmentation result on various B-scans. The layers/boundaries marked are (from top): ILM, NFL-GCL, IPL-INL, OPL-ONL, IS/OS, OS, OPR and RPE

4.3 Three Dimensional Image Segmentation of Retinal OCT Image using Intensity / Threshold Information

Three dimensional macular OCT image provides better visualization of tissue structures. In two dimensional processing of macular OCT images, the possibility of error in matching layers in between adjacent cross-sectional images is high. Moreover three dimensional processing compensates for the error due shadowed region caused by blood vessels or any other information loss. This segmentation has utilized the intensity profile of macular OCT images to divide the macular scan in to three regions [Figure 4.1]. The ONL to IS region has significantly lower intensity level compared to ILM to OPL region on top and OS to BM in bottom. These three regions are used for limiting search region in segmentation algorithm. The layers and boundaries are detected by utilizing their intensity profile and the order of occurrence in macular OCT image. Figure 4.6 shows the flowchart of intensity based segmentation process.

4.3.1 Denoising and Finding Area of Interest

The macular OCT images are arranged in a three dimensional data cube i.e. $1024 \times 512 \times 128$ $(Z \times X \times Y)$. Denoising is performed in order to remove speckle noise and smoothen the intensity variation of image. Gaussian filter of size 5×7 and SD 2 is used to filter each cross-sectional image. In the Gaussian filtered data, each A-scan is then processed to remove DC component in them. Figure 4.7 shows the intensity variation in A-scan. Red colored line shows the actual intensity variation, blue colored line shows intensity variation in Gaussian filtered image and green colored line shows intensity variation when dc component in each A-scan is removed and A-scans are normalized. To reduce the memory usage of computer, vitreous and choroid regions are removed. Anterior boundary is obtained by converting each cross-sectional image into binary form with threshold 0.1. The first white pixel in each A-scan is marked as anterior boundary.
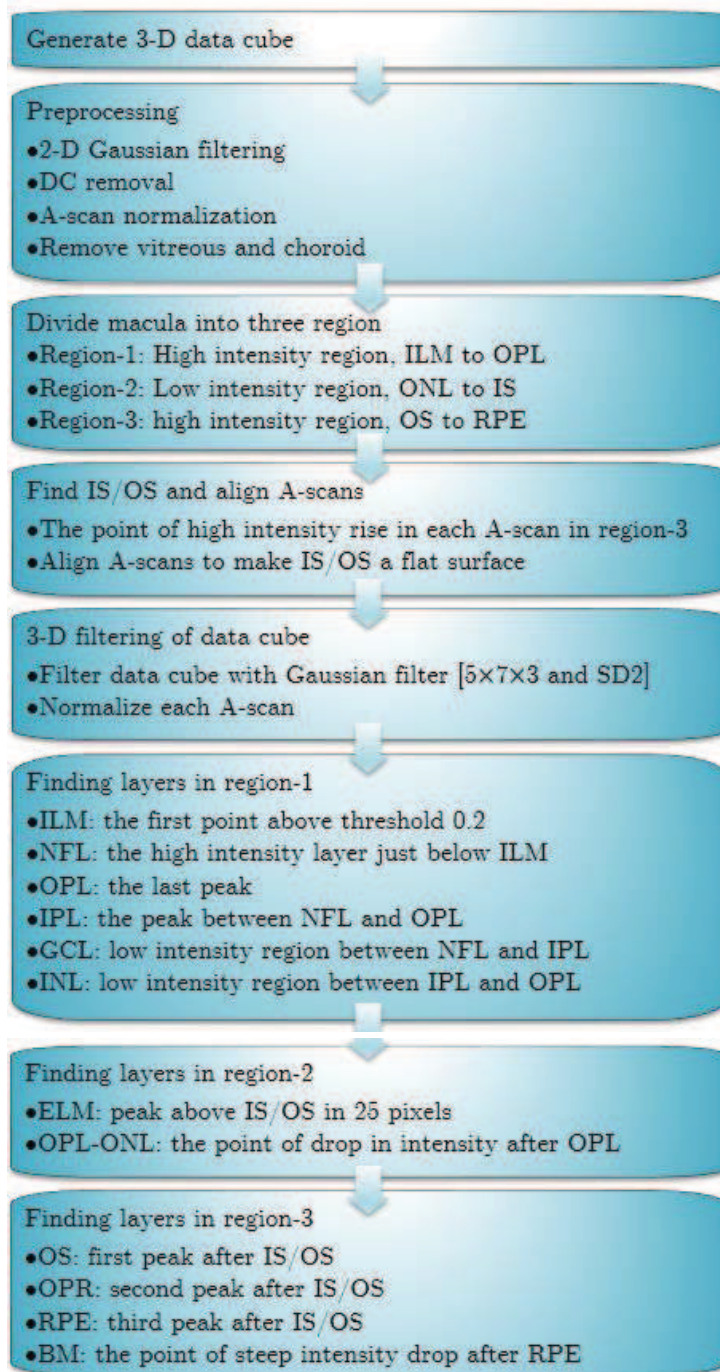
Figure 4.6: Flow chart of intensity based segmentation algorithm

To obtain posterior boundary, each cross-sectional image is converted to binary image with threshold 0.3 and first white pixel from choroid to vitreous direction is marked as posterior boundary. The XY planes before anterior boundary and after posterior boundary are removed. Figure 4.8 shows (a) the original macular OCT image and (b) when vitreous and choroid region are removed.
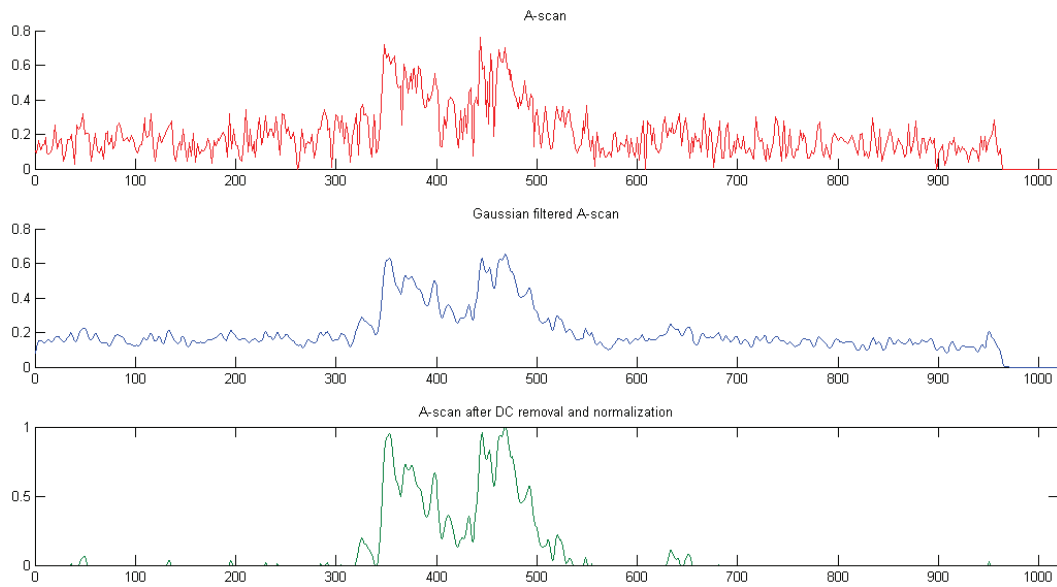
Figure 4.7: Intensity variation in a A-scan in original image (red), Gaussian filtered image (blue); and when DC part is removed and A-scan is normalized (green)

4.3.2 Separating Macular Image in Three Regions

In macular OCT image, the intensity of ONL is lower compared to NFL, INL IPL on top and OS, RPE in bottom. These intensity characteristic is used to divide macular cube in three sections. Region-1 contains ILM, NFL, GCl, IPl, INL and OPL. Region-2 contains ONL, ELM and IS. And region-3 contains OS, OPR, RPE and Bruch membrane. To get these three regions, data cube was multiplied with a three dimensional matrix of size 7×5×5 with each element value one. The resultant was normalized and converted to binary form with threshold 0.3. In the resultant binary images, the upper and lower high intensity pixels in binary form are marked as region-1 and region-3 respectively, with region-2 between them as shown in Figure 4.8(c).
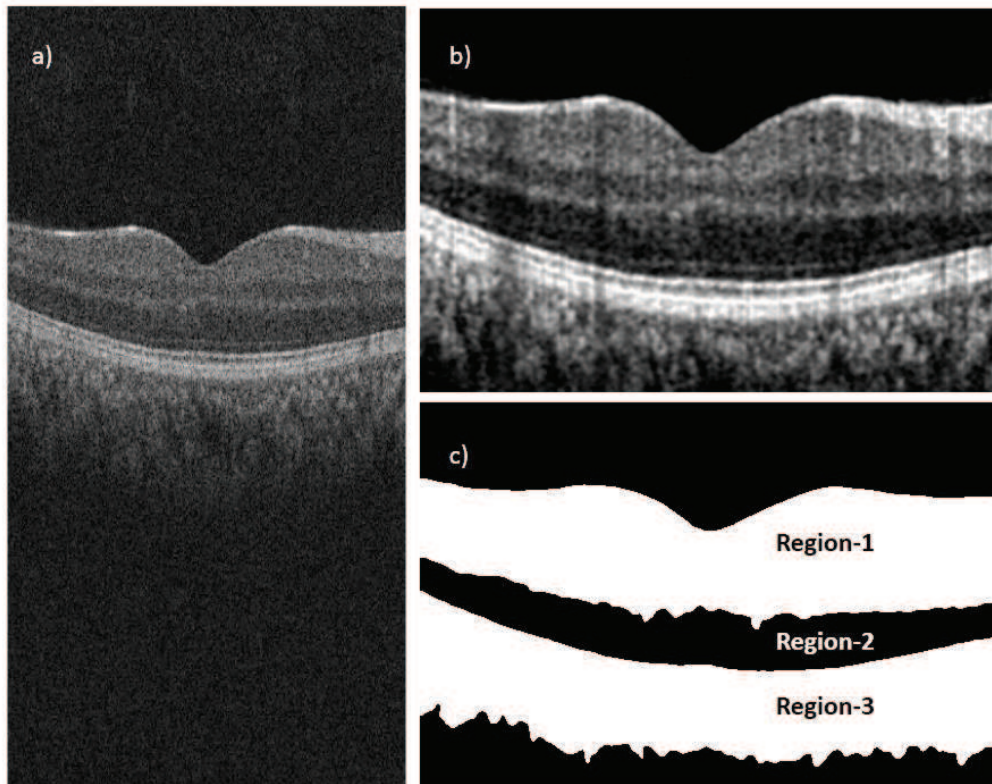
Figure 4.8: a) one cross-sectional OCT scan of macula. b) Vitreous and choroid regions are removed from OCT image. c) OCT image divided into three regions.

4.3.3 Aligning A-scans along IS/OS

In region-3, IS/OS show the first intensity rise. So the first intensity rise in region-3 is marked as IS/OS. Thus obtained IS/OS boundary is further smoothened with help of axial gradient information. All A-scan are aligned to make IS/OS a straight line. 3-D filtering of thus obtained data cube is performed in order to smooth the intensity variation in adjacent cross-sectional image. Three-dimensional filtering should be performed after A-scan alignment because in original dataset there may be misalignment between B-scans. In the shadowed region due to blood vessels, this process fills in the intensity information from neighboring pixels. A Gaussian matrix of size $5 \times 7 \times 3$ and SD 2 is used for this process. Each A-scan is normalized. As the OCT images are obtained with A-scan as its unit, normalization helps in generalizing the parameters used to find various layers. The Second normalization in region-3 helped in minimizing error in shadowed regions. Figure 4.9 shows (a) the OCT image flattened along IS/OS and (b) same image after 3-D filtering. Red arrows in Figure 4.9(a) points at high scattering near ILM layer due to blood vessels. The boxes below them show the shadowed region. After 3-D filtering and normalization, the error due to blood vessels is considerably minimized as shown in Figure 4.9(b). Now preprocessing part of segmentation algorithm is over. This 3-D smoothened data cube will be used to find

34

the different macular layers according to their intensity profile. The intensity variation of A-scan used to find layers is shown in Figure 4.1.
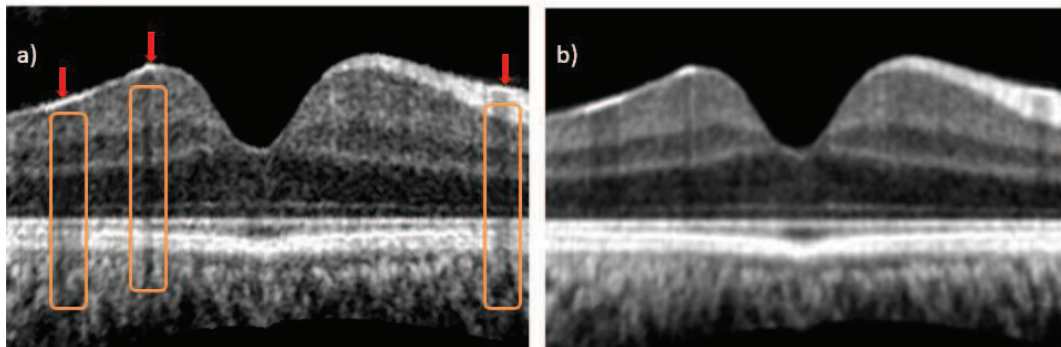
Figure 4.9: a) OCT image flattened along IS/OS. b) Same image after 3-D filtering. [Red arrows shows high scattering due to blood vessels and behind them are shadowed region in boxes]

4.3.4   Finding Macular Layers

Retinal layers are obtained from flattened and 3-D filtered data cube with help of three regions marked in step 4.3.2. Region-1 has three peaks, NFL, IPL and OPL. The average pixel intensity is around 0.4 to 0.5. In region-2, the average pixel intensity is about 0.2. The average pixel intensity again increases in region-3 and is about 0.7 to 0.8.

Region-1:

Inner Limiting Membrane (ILM): Inner limiting membrane separates macular tissue form viscous and transparent vitreous fluid. At this junction, the intensity of backscattered light increases sharply. In each A-scan, ILM is marked as the first pixel above threshold of 0.2. The algorithm process is limited in region1 and direction is from vitreous to choroid.

Nerve Fiber Layer (NFL): Nerve fiber layer is the brighter region attached to ILM. The NFL is marked as the pixels, just after ILM, with pixel value threshold of 0.6.

Outer Plexiform Layer (OPL): On the other side of region-1, ONL to OPL transition has intensity rise similar as to intensity rise from vitreous to ILM. OPL layer is marked as the peak just at end of region-1 in each A-scan.

Inner Plexiform Layer (IPL): The inner plexiform layer is marked by finding the peak in between NFL and OPL.

Ganglion Cell Layer (GCL): Ganglion cell layer is the layer between NFL and IPL. It has lower intensity compared to NFL and IPL. GCL is marked as lower intensity region between NFL and IPL.

Inner Nuclear Layer (INL): Inner nuclear layer is the low intensity region between IPL and OPL. INL is obtained by comparing the intensity drop between IPL and OPL.

Region-2:

Region-2 contains ONL, ELM and IS. It has relatively low pixel intensity compared to region-1 and region-2.

External Limiting Membrane (ELM): External limiting membrane is layer of relatively high intensity in region-2 and is just above IS/OS. ELM is marked by finding the pixel of peak value in window of 25 pixels just above IS/OS.

Outer Nuclear Layer (ONL): Outer nuclear layer is the wide region of low intensity between OPL and ELM. The OPL-ONL boundary is detected as the point of drop in intensity after OPL.

Region-3:

Region-3 is the brightest among all. It contains OS, OPR, RPE and Bruch's membrane.

Outer Photoreceptor Segment (OS): OS is marked as the first peak in region-3.

Outer Segment PR/RPE complex (OPR): OPR is marked as second peak in region-3, i.e. after OS.

Retinal Pigment Epithelium (RPE): RPE is marked as third peak in region-3, i.e. after OPR.

Bruch's Membrane (BM): There is sharp decline in pixel intensity at BM. The point of sharp drop in pixel intensity after RPE in region-3 is marked as BM.

The different boundaries are filtered with a modified median filter. The segmentation results overlapped on original OCT images is shown in Figure 4.10.Segmentation result from top: ILM, NFL-GCL, GCL-IPL, IPL-INL, INL-OPL, OPL-ONL, ELM, IS/OS, OPR, RPE, Bruch's membrane. Figure 4.11 shows the three dimensional view of segmented layers of retina. The layers are shown at a distance from each other for proper visualization. The layers are (from top): NFL, GCL, IPL, INL, OPL, ONL-ELM, ELM-IS/OS, OS, OPR and RPE.
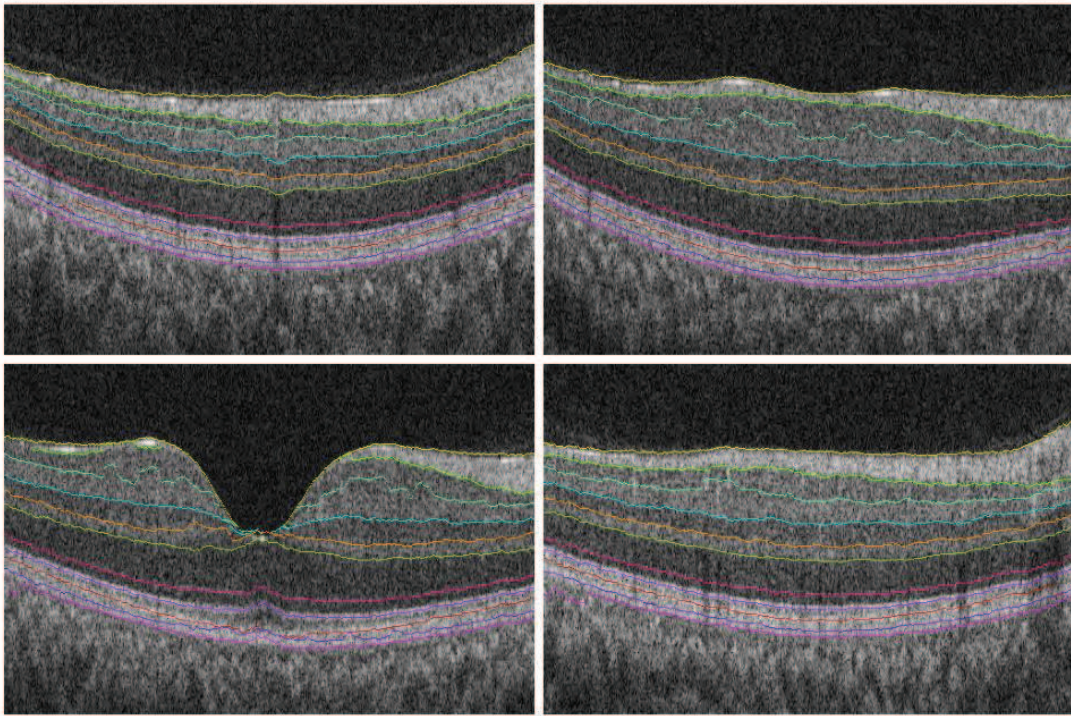
Figure 4.10: The segmentation results showed on original OCT images. Segmentation result from top: ILM, NFL-GCL, GCL-IPL, IPL-INL, INL-OPL, OPL-ONL, ELM, IS/OS, OPR, RPE, Bruch's membrane.
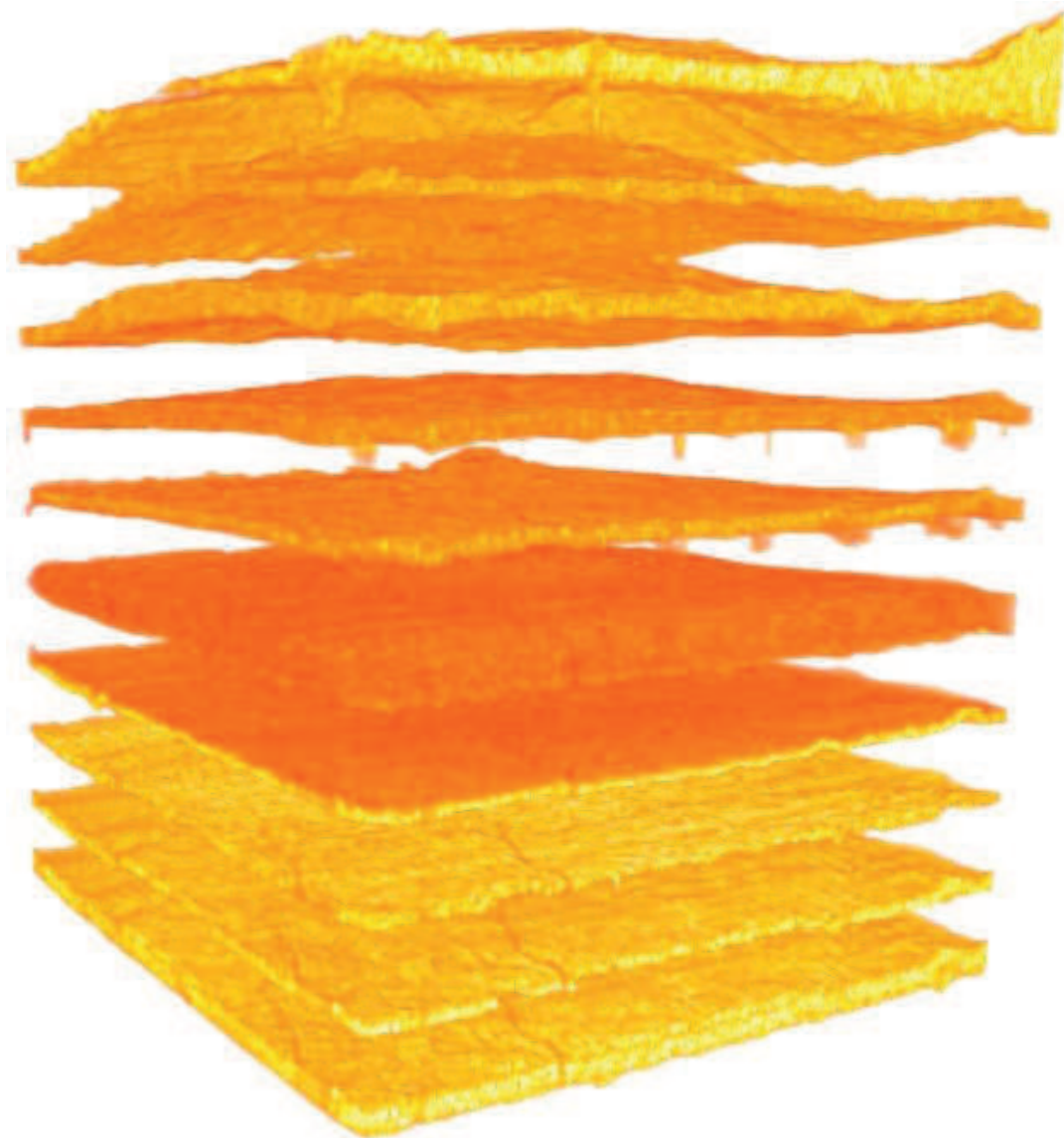
Figure 4.11: shows the different layers of macula as obtained in segmentation. From top: NFL, GCL, IPL, INL, OPL, ONL-ELM, ELM-IS/OS, OS, OPR, and RPE.

4.3.5   Macular Analysis

4.3.5.1. Find Fovea Center and Display Two Cross-section images at Fovea

At fovea, the A-scans have less total intensity i.e. addition of all pixels of A-scan. The normalized A-scan sum matrix was converted to binary form with threshold .5. In black region of this binary image, fovea location was obtained as the point of ILM and RPE difference. Figure 4.12 shows the two mutually cross-sectional images at center of fovea (259, 64). And the minimum ILM-RPE thickness at the center for given image was 207 μm.
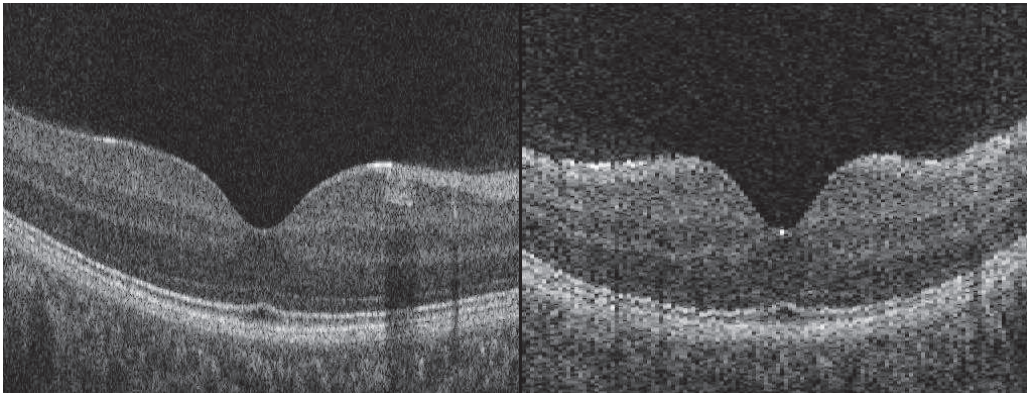
Figure 4.12: shows the two mutually cross-sectional images at center of fovea

4.3.5.2. Display ILM and RPE, and RPE Fit-Function

Figure 4.13 shows the ILM (top) and RPE (below) layers.
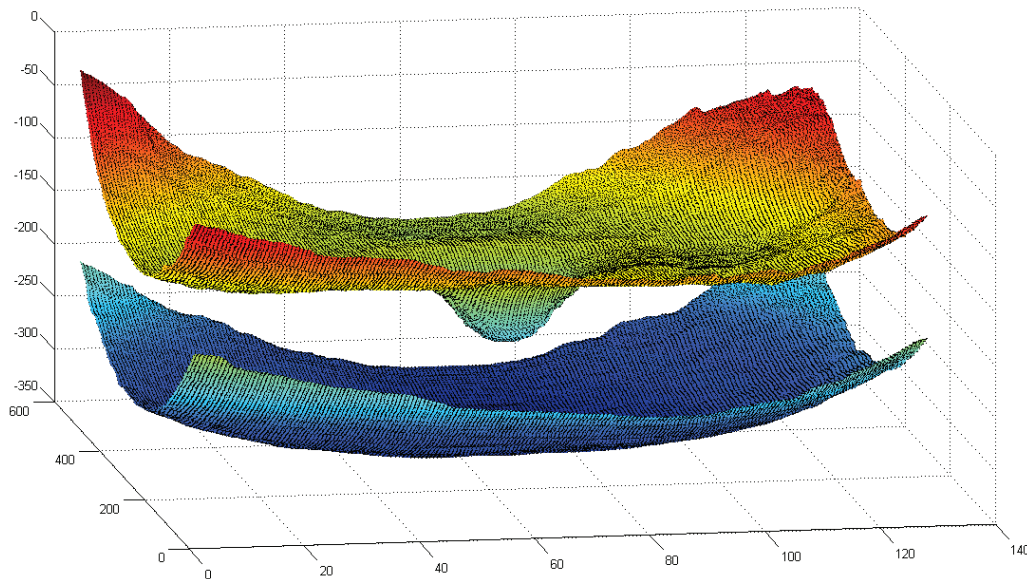
Figure 4.13: shows the ILM (top) and RPE (below) layers.

RPE fit function displays the ILM by making RPE is a flat surface. So it is essentially the ILM-RPE thickness plot. Figure 4.14 shows the RPE-fit function plot.

Macular cube average thickness:

(RPE-ILM)×(1024 ÷ 2000) μm = 285.16μm.

The macular cube volume measured as the macular volume between ILM and RPE for the ILM-RPE layer show above is:

(Average (ILM-RPE))÷ 1024 × 2 × 6 × 6 mm^3= 10.23mm^3
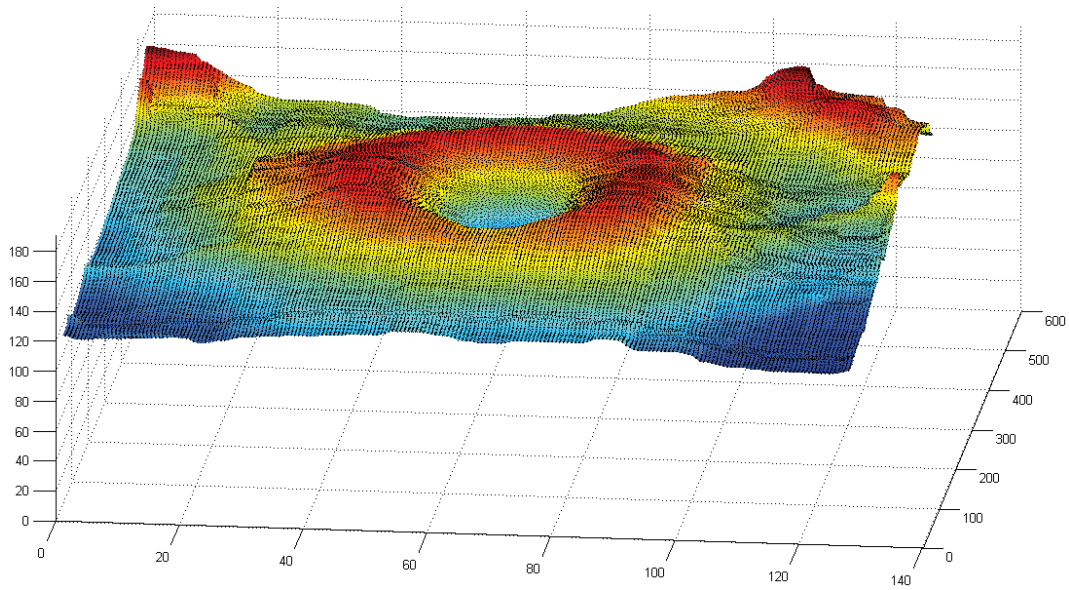
Figure 4.14: shows the RPE- fit function plot

Table 4.1: ILM-RPE analysis

	Central Subfield Thickness (μm)	Cube Volume (mm^3)	Cube Average Thickness (μm)
RPE	257.23	10.23	285.16

Table 4.1 shows the ILM-RPE analysis. Figure 4.15 shows the ILM-RPE thickness variation on macular surface.

Fovea Location (259, 64)   ILM-RPE thickness (μm)   ILM-RPE Fit Plot
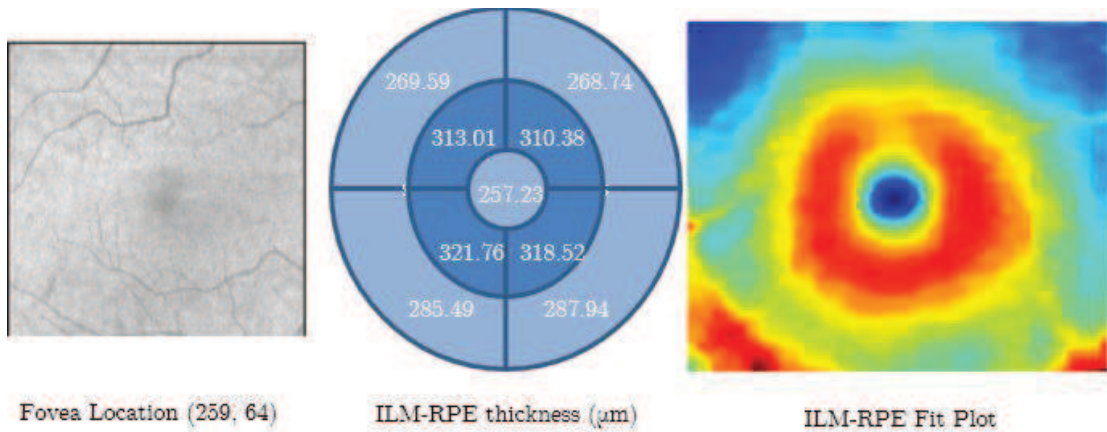
Figure 4.15: shows the ILM-RPE thickness variation on macular surface

Chapter 5
Summary, Conclusion and Future Work

5.1 Summary

The two algorithms were applied on 15 macular OCT cube of dimension 1024×512×128 obtained from healthy volunteers using Cirrus HD-OCT system. In 2-dimensional gradient based segmentation algorithm, five layer boundaries: ILM, NFL-GCL, IPL-INL, OPL-ONL and IS/OS; and three retinal layers: OS, OPR and RPE were successfully obtained. The time required to process the complete data cube of size 1024×512×128 was 43 seconds. The RPE detection was made easier by first locating IS/OS, which eliminated the need of iterative statistical regression method [18] or any other error correction [16].

3-dimensional intensity based segmentation algorithm used intensity characteristic of macular OCT scan to mark various layers and layer boundaries. In this, eight macular layer boundaries: ILM, NFL-GCL, GCL-IPL, IPL-INL, INL-OPL, OPL-ONL, IS/OS and BM; and three layers ELM, RPE, and OPR were segmented. The 3-D filtering of data cube greatly reduced the error in shadowed region behind blood vessels. The program took 38 seconds to complete segmentation. Macula was divided into three regions based on intensity. These regions were used to limit search region in locating boundaries. Uniform intensity variation in A-scan was obtained by 3-D filtering and then normalizing each A-scan. The search parameters for each layer were constant throughout the macular cube as intensity variation in macular cube was homogenized. The parameters used to locate boundaries were optimized for Cirrus HD-OCT system.

5.2 Conclusion

An automated three-dimensional macular OCT image segmentation has been developed and evaluated. The segmentation algorithm used characteristic intensity profile of macular OCT image to locate various boundaries and layers. The division of macular cube in three regions based on intensity considerably reduced the processing time and error in boundary location. The 3-D filtering performed on data cube compensated for the information loss in shadowed regions and smoothened the intensity variation between B-scans. Uniformed intensity of macular cube helped in generalizing parameters set for various layers. The segmentation process was simplified and generalized with the help of two factors: separating the macula in three regions of interest and homogenized intensity variation throughout macular cube.

5.3 Future Work

Further study needs to be performed on testing and optimizing proposed algorithm on macular scans in various ocular disease conditions. The gradient information can be used

simultaneously to enhance the accuracy in locating boundaries and to evaluate various layer thicknesses. The program should be made to provide quantitative analysis of macula and to suggest possible disease condition.

References

1. Bruno, L. and R. Marco, *Guide to Interpreting Spectral Domain Optical Coherence Tomography*. 2011: JAYPEE BROTHERS PUBLISHERS.
2. Huang, D., et al., *Optical coherence tomography.* Science, 1991. **254**(5035): p. 1178-1181.
3. Stevens, T.S., *OPtical coherence tomography of ocular diseases, 2nd ed.* Archives of Ophthalmology, 2005. **123**(2): p. 292-292.
4. Regar, E., A. van Leeuwen, and P.W. Serruys, *Optical coherence tomography in cardiovascular research*. 2007: CRC Press.
5. Drexler, W. and J.G. Fujimoto, *Optical coherence tomography: technology and applications*. 2008: Springer.
6. Potsaid, B., et al., *Ultrahigh speed spectral/Fourier domain OCT ophthalmic imaging at 70,000 to 312,500 axial scans per second.* Optics express, 2008. **16**(19): p. 15149-15169.
7. Choma, M., et al., *Sensitivity advantage of swept source and Fourier domain optical coherence tomography.* Optics Express, 2003. **11**(18): p. 2183-2189.
8. De Boer, J.F., et al., *Improved signal-to-noise ratio in spectral-domain compared with time-domain optical coherence tomography.* Optics letters, 2003. **28**(21): p. 2067-2069.
9. Leitgeb, R., C. Hitzenberger, and A. Fercher, *Performance of fourier domain vs. time domain optical coherence tomography.* Optics Express, 2003. **11**(8): p. 889-894.
10. Cense, B., et al., *Ultrahigh-resolution high-speed retinal imaging using spectral-domain optical coherence tomography.* Optics Express, 2004. **12**(11): p. 2435-2447.
11. Leitgeb, R., et al., *Real-time assessment of retinal blood flow with ultrafast acquisition by color Doppler Fourier domain optical coherence tomography.* Optics Express, 2003. **11**(23): p. 3116-3121.
12. Makita, S., et al., *Optical coherence angiography.* Optics Express, 2006. **14**(17): p. 7821-7840.
13. Vakoc, B., et al., *Phase-resolved optical frequency domain imaging.* Optics Express, 2005. **13**(14): p. 5483-5493.
14. White, B., et al., *In vivo dynamic human retinal blood flow imaging using ultra-high-speed spectral domain optical coherence tomography.* Optics Express, 2003. **11**(25): p. 3490-3497.
15. Wojtkowski, M., et al., *Ultrahigh-resolution, high-speed, Fourier domain optical coherence tomography and methods for dispersion compensation.* Optics express, 2004. **12**(11): p. 2404-2422.
16. Fabritius, T., et al., *Automated segmentation of the macula by optical coherence tomography.* Optics Express, 2009. **17**(18): p. 15659-15669.
17. Yang, Q., et al., *Automated layer segmentation of macular OCT images using dual-scale gradient information.* Optics Express, 2010. **18**(20): p. 21293-21307.

18. Zhang, X., et al., *Automated segmentation of intramacular layers in Fourier domain optical coherence tomography structural images from normal subjects.* J Biomed Opt, 2012. **17**(4): p. 046011.

19. Yazdanpanah, A., et al., *Intra-retinal Layer Segmentation in Optical Coherence Tomography Using an Active Contour Approach*, in *Medical Image Computing and Computer-Assisted Intervention – MICCAI 2009*, G.-Z. Yang, et al., Editors. 2009, Springer Berlin Heidelberg. p. 649-656.

20. Mishra, A., et al., *Intra-retinal layer segmentation in optical coherence tomography images.* Optics Express, 2009. **17**(26): p. 23719-23728.

21. Garvin, M.K., et al., *Automated 3-D Intraretinal Layer Segmentation of Macular Spectral-Domain Optical Coherence Tomography Images.* Medical Imaging, IEEE Transactions on, 2009. **28**(9): p. 1436-1447.

22. Dufour, P.A., et al., *Graph-Based Multi-Surface Segmentation of OCT Data Using Trained Hard and Soft Constraints.* Medical Imaging, IEEE Transactions on, 2013. **32**(3): p. 531-543.

23. Chiu, S.J., et al., *Automatic segmentation of seven retinal layers in SDOCT images congruent with expert manual segmentation.* Optics Express, 2010. **18**(18): p. 19413-19428.

24. Chiu, S.J., et al., *Validated automatic segmentation of AMD pathology including drusen and geographic atrophy in SD-OCT images.* Invest Ophthalmol Vis Sci, 2012. **53**(1): p. 53-61.

25. Vermeer, K.A., et al., *Automated segmentation by pixel classification of retinal layers in ophthalmic OCT images.* Biomedical Optics Express, 2011. **2**(6): p. 1743-1756.

26. AHMAD, K.M., et al., *Cell density ratios in a foveal patch in macaque retina.* Visual neuroscience, 2003. **20**(02): p. 189-209.

27. Kolb, H. *Simple Anatomy of the Retina* Available from: http://webvision.med.utah.edu/book/part-i-foundations/simple-anatomy-of-the-retina/.

28. De Jong, P.T., *Age-related macular degeneration.* New England Journal of Medicine, 2006. **355**(14): p. 1474-1485.

29. Casson, R.J., et al., *Definition of glaucoma: clinical and experimental concepts.* Clinical & experimental ophthalmology, 2012. **40**(4): p. 341-349.

30. *Cirrus HD-OCT Model 400 - Carl Zeiss Meditec*.